Zhao *et al. Microstructures* **2025**, *5*, 2025034
DOI: 10.20517/microstructures.2024.128

Microstructures

Review

Open Access

Recent advances of two-dimensional molybdenum oxides

Zeyuan Zhao[1,#], Weimin Lei[2,#], Tianyu Zhou[1], Kang Chen[3], Kaiwen Tian[1], Gaojie Xiong[1], Shuangyang Kuang[1], Liwei Xiong[1], Yiling Yu[4], Liang Huang[3]

[1]Hubei Key Laboratory of Plasma Chemistry and Advanced Materials, School of Materials Science and Engineering, Wuhan Institute of Technology, Wuhan 430205, Hubei, China.
[2]School of Power and Mechanical Engineering, Wuhan University, Wuhan 430072, Hubei, China.
[3]Wuhan National Laboratory for Optoelectronics, School of Optical and Electronic Information, Huazhong University of Science and Technology, Wuhan 430074, Hubei, China.
[4]School of Physics and Technology, Wuhan University, Wuhan 430072, Hubei, China.
[#]Authors contributed equally.

Correspondence to: Prof. Shuangyang Kuang, Hubei Key Laboratory of Plasma Chemistry and Advanced Materials, School of Materials Science and Engineering, Wuhan Institute of Technology, 206 Guanggu 1st Road, Wuhan 430205, Hubei, China. E-mail: 22041201@wit.edu.cn; Prof. Liwei Xiong, Hubei Key Laboratory of Plasma Chemistry and Advanced Materials, School of Materials Science and Engineering, Wuhan Institute of Technology, 206 Guanggu 1st Road, Wuhan 430205, Hubei, China. E-mail: zhily2000@126.com; Prof. Yiling Yu, School of Physics and Technology, Wuhan University, 299 Bayi Road, Wuhan 430072, Hubei, China. E-mail: yilingyu@whu.edu.cn; Prof. Liang Huang, Wuhan National Laboratory for Optoelectronics, School of Optical and Electronic Information, Huazhong University of Science and Technology, 1037 Luoyu Road, Wuhan 430074, Hubei, China. E-mail: huangliang421@hust.edu.cn

How to cite this article: Zhao, Z.; Lei, W.; Zhou, T.; Chen, K.; Tian, K.; Xiong, G.; Kuang, S.; Xiong, L.; Yu, Y.; Huang, L. Recent advances of two-dimensional molybdenum oxides. *Microstructures* **2025**, *5*, 2025034. https://dx.doi.org/10.20517/microstructures.2024.128

Received: 18 Nov 2024 **First Decision:** 11 Jan 2025 **Revised:** 16 Jan 2025 **Accepted:** 25 Jan 2025 **Published:** 24 Mar 2025

Academic Editor: Yi Du **Copy Editor:** Fangling Lan **Production Editor:** Fangling Lan

Abstract

Over two decades have passed since the successful exfoliation of graphene, which initiated the exploration of two-dimensional (2D) materials. Since then, this vibrant group has expanded to encompass a variety of new materials. Among these, molybdenum (Mo)-based oxides with 2D structures have attracted growing interest. Due to their remarkable properties, 2D Mo-based oxides have ensured their prominent position in cutting-edge scientific domains, including energy applications, catalysis and electronic devices. This review systematically examines recent advancements in the synthesis, structural regulation, and applications of 2D Mo-based oxides. Firstly, a detailed overview of various synthesis techniques is given, including but not limited to hydrothermal methods, physical vapor deposition, and chemical vapor deposition, enabling the production of high-quality 2D Mo-based oxides. Subsequently, strategies are presented for structural regulation through doping, interface engineering, and

interlayer tuning. Finally, recent application developments in energy conversion and storage, catalysis, sensing, and optoelectronic devices are highlighted. Furthermore, an outlook on potential future trends is provided at the conclusion of the review, aiming to advance the practical deployment of 2D Mo-based oxides in emerging technologies.

Keywords: Two-dimensional (2D) materials, molybdenum oxides, nanostructure, structural regulation

INTRODUCTION

With the ongoing advancement of research efforts, two-dimensional (2D) materials have achieved remarkable progress and become a highlight in the field of materials science. Graphene, transition metal chalcogenides, black phosphorus, hexagonal boron nitride (h-BN), and MXenes are widely acknowledged as representative 2D materials, each exhibiting unique physicochemical properties that have revolutionized fields such as electronics, catalysis, and energy storage. These materials have established high standards for low-dimensional systems due to their exceptional electronic, optical, and mechanical properties.

Notably, the exploration of 2D materials is not limited to these well-studied systems. Metal oxides, a class of materials with diverse compositions and functionalities, have also garnered significant attention in recent years. Metal oxides, including transition metal oxides and rare earth metal oxides, are traditionally known for their stability, tunable electronic properties, and redox activity[1]. These properties make them indispensable in applications ranging from catalysis to energy storage. While bulk and nanoparticle forms of metal oxides have been extensively investigated, their 2D counterparts offer distinct advantages, such as enhanced specific surface area, improved charge transport properties, and the ability to precisely engineer electronic properties through compositional and structural regulation[2].

Despite these advantages, the development of 2D metal oxides faces several challenges. For instance, the synthesizing of high-quality, large-area 2D metal oxides with precise control over thickness and composition remains a significant hurdle. Additionally, the fundamental understanding of 2D metal oxide structure-property relationships, particularly in comparison to their bulk counterparts, is still incomplete. These gaps hinder the full exploitation of their potential in practical applications.

Among the emerging 2D metal oxides, molybdenum (Mo)-based oxides have recently emerged as a promising subcategory. These materials combine the inherent advantages of metal oxides with the unique characteristics of 2D structures, such as tunable bandgaps, robust redox activity, and distinctive electrical and optical properties. These attributes position 2D Mo-based oxides as potential candidates for addressing pressing global challenges, including energy scarcity and environmental contamination. For instance, high surface area and active sites make them ideal for catalytic applications, while their tunable electronic properties are advantageous for energy storage and optoelectronic devices.

However, despite their potential, research on 2D Mo-based oxides is still in its early stages. Several critical challenges remain unresolved, including the development of effective synthesis methods for producing high-quality 2D Mo-based oxides, the precise tuning of their electronic and optical properties to meet specific application requirements, and the identification of key factors governing their performance in energy storage and catalytic applications. Addressing these questions is essential for unlocking the full potential of 2D Mo-based oxides and advancing their practical applications.

In this context, this review aims to provide a comprehensive overview of the latest research developments in 2D Mo-based oxides. The article will systematically discuss the various synthesis methods, strategies for structural regulation, and applications in fields such as catalysis, energy storage, and optoelectronics [Figure 1]. Furthermore, we will highlight the challenges and future directions for 2D Mo-based oxides, offering insights into their potential to drive innovations in materials science and technology. By addressing the existing research gaps and providing a roadmap for future research, this review aims to inspire further exploration and accelerate the development of 2D Mo-based oxides for practical applications.

STRUCTURE AND PROPERTIES OF MO-BASED OXIDES

Two-dimensional Mo-based oxides can be classified into two categories based on their structure: layered and non-layered. Molybdenum trioxide (MoO_3) belongs to the layered structures, while molybdenum dioxide (MoO_2) is classified as the non-layered structures. Layered structures consist of multiple atomic planes stacked together, with layers weakly interacting via van der Waals forces while being strongly bonded through covalent interactions within the plane. These materials can be reduced to atomic thicknesses without compromising their crystalline quality. In contrast, non-layered structures tend to grow laterally while being confined vertically, leading to some exposed Mo or oxygen atoms at the edges that are not fully bonded, thus creating unsaturated dangling bonds[3]. These structural differences lead to significant variations in the physical and chemical properties of the materials, thereby influencing their applicability. Layered structures are noted for their exceptional mechanical robustness and optical performance, rendering them particularly advantageous for integration into electronic and optoelectronic devices. Meanwhile, non-layered structures are primarily exploited for their catalytic activity and potential in energy storage systems.

MoO_3

MoO_3 is an important transition metal oxide that naturally occurs in the form of molybdenite and is generally observed as being white or colorless. Its crystalline forms include α-MoO_3, β-MoO_3, ε-MoO_3, and h-MoO_3[4], with the thermodynamically stable orthorhombic phase (α-MoO_3) being the most widely studied and utilized. The α-MoO_3 exhibits a unique 2D layered structure, as illustrated in Figure 2A and B. In α-MoO_3, MoO_6 octahedra are arranged in bilayers, where one MoO_6 octahedral layer shares edges with another MoO_6 octahedral layer. Within each layer, the interatomic distance between Mo atoms is approximately 0.7 nm, while the distance between Mo atoms in adjacent layers is around 1.4 nm[5]. This structure confers MoO_3 with notable anisotropy in its physical properties, such as thermal conductivity and optical characteristics, which vary depending on the crystal orientation.

As an n-type semiconductor, MoO_3 is characterized by a wide bandgap, high electron affinity, and high ionization energy. When present in reduced oxidation states, such as MoO_{3-x}, defect states can form within the bandgap, leading to a color change from transparent to yellow or even blue-gray. This photochromic property renders it suitable for applications in photochromic devices[6].

Recent studies have highlighted 2D α-MoO_3 as a natural material for hyperbolic phonon polaritons (PhPs). α-MoO_3 demonstrates significant in-plane optical anisotropy, which allows it to support hyperbolic PhPs in the mid-infrared region. These properties result in strong spatial confinement effects and lower losses, positioning α-MoO_3 as an ideal platform for investigating new optical phenomena[7-9]. Furthermore, the tunable localized surface plasmon resonance (LSPR) effect exhibited by 2D MoO_3, coupled with its active performance in twistronics and near-field radiative heat transfer, highlights its substantial potential for a wide range of applications[10-16].

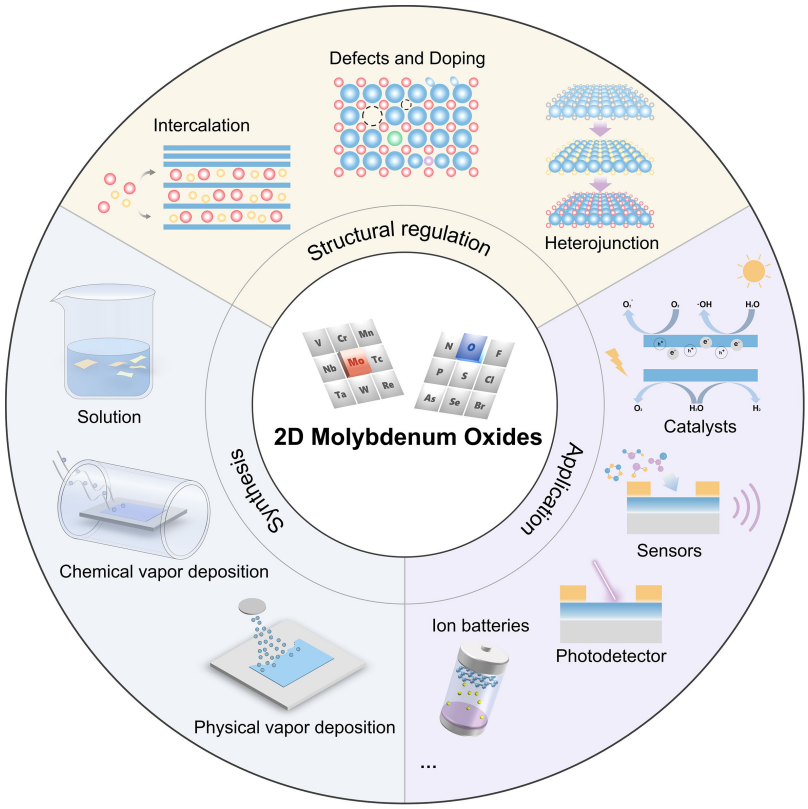

Figure 1. Schematic overview of synthesis strategies, structural regulation, and applications of 2D molybdenum oxides.

MoO_2

MoO_2 adopts a monoclinic crystal structure (space group $P2_1/c$), which bears similarities to the rutile structure. Rutile, which belongs to the tetragonal system, is characterized by a metal center coordinated with six oxygen atoms, forming an octahedral environment. Each oxygen atom is bonded to three metal atoms at the vertices of an equilateral triangle, thereby maintaining a uniform metal-metal bond length[17].

In contrast, MoO_2 exhibits a distorted crystal structure, where MoO_6 octahedra are linked by shared edges along the [001] direction [Figure 2C]. This distortion leads to an alternation in Mo-Mo bond lengths along the rutile c-axis, with values of 2.51 and 3.02 Å. Consequently, two distinct oxygen coordination environments are created, each with three different M-O bond lengths [Figure 2D][18].

The differing crystal structures of MoO_2 and MoO_3 give rise to variations in the orbitals occupied by valence electrons, which in turn affects their electronic properties. MoO_3 is an n-type semiconductor due to its electronic structure, whereas MoO_2 exhibits metallic conductivity[19]. Despite these differences, phase transitions between MoO_2 and MoO_3 can occur through electron migration, such as the conversion of MoO_2 into MoO_3.

SYNTHESIS METHODS

The novel properties of 2D Mo-based oxides and their potential applications in numerous fields have drawn significant attention, driving rapid advancements in synthetic strategies. Obtaining stable and high-quality 2D films or nanosheets remains challenging. Generally, synthesis methods can be categorized into top-down and bottom-up approaches[20].

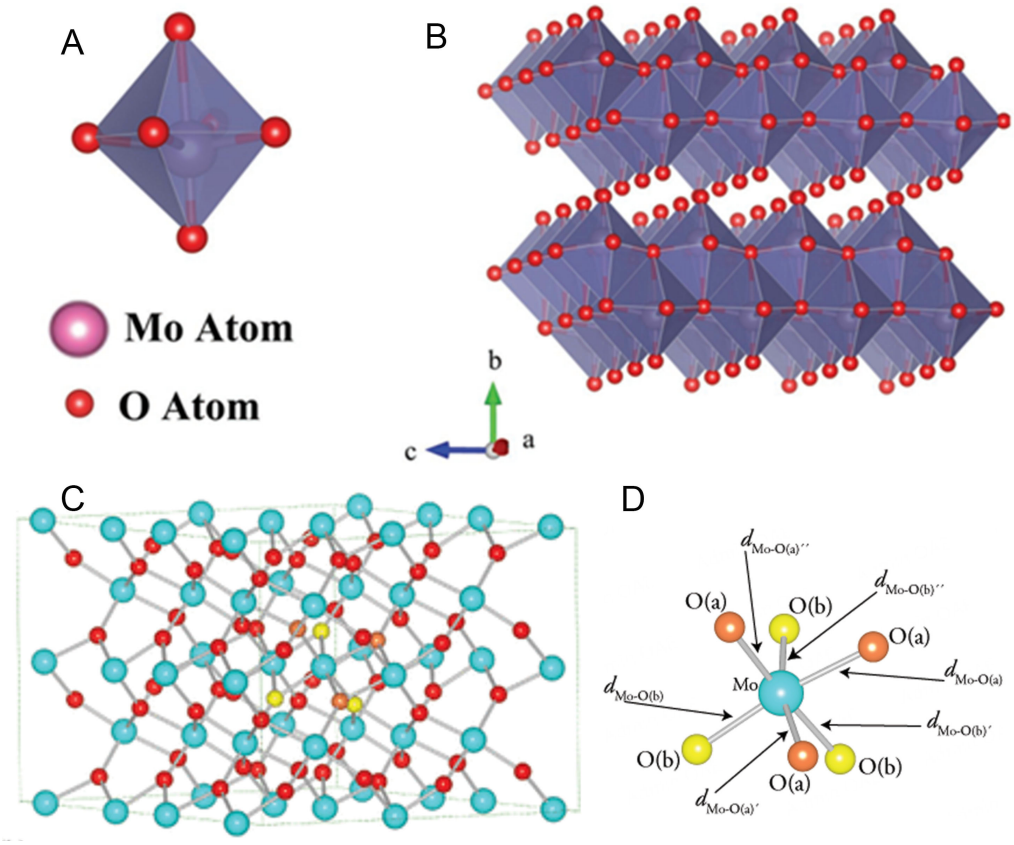

Figure 2. (A) MoO_6 octahedra as found in the thermodynamically stable α-MoO_3 composed of molybdenum and oxygen atoms. (B) Thermodynamically stable orthorhombic α-MoO_3 with layered structure held together by van der Waals' forces. (C) Crystal structure of monoclinic MoO_2. (D) MoO_6 distorted octahedra highlighting the bond ordering. (A and B) reprinted with permission[5]. Copyright 2017, Wiley-VCH. (C and D) reprinted with permission[18]. Copyright 2010, American Chemical Society.

Top-down strategies

Top-down strategies begin at the macroscopic level and involve the use of physical or chemical means to exfoliate monolayer or few-layer nanosheets from bulk materials. Common 2D materials exfoliation techniques encompass mechanical exfoliation, liquid-phase exfoliation, chemical exfoliation, and electrochemical exfoliation. For 2D Mo-based oxides, this section will focus on two prominent exfoliation methods that have garnered significant attention in recent years: liquid-phase exfoliation and supercritical CO_2-assisted exfoliation. Table 1 summarizes the advantages and limitations of these various exfoliation techniques. While mechanical exfoliation is often the most straightforward and efficient method to obtain layered 2D materials, the lack of dimensional control renders it unsuitable for large-scale synthesis.

Compared to traditional mechanical exfoliation, liquid-phase exfoliation offers advantages in terms of yield and the elimination of repetitive operations. The process of liquid-phase exfoliation involves several steps, including mechanical grinding, ultrasonic treatment, and centrifugal separation. These steps are designed to disrupt the interlayer van der Waals forces, thereby facilitating the exfoliation of large-area layered materials into individual or few-layer nanosheets. Furthermore, by adjusting the type of exfoliating solvent and processing conditions, such as temperature and duration, the performance of the nanosheets can be further optimized.

Table 1. Comparison of various exfoliation methods for 2D Mo-based Oxides

Technique	Advantages	Limitations
Mechanical exfoliation	High-quality, defect-free monolayers Simple and cost-effective No chemical contamination	Low yield and poor thickness control Not scalable
Liquid-phase exfoliation	Higher yield than mechanical exfoliation Scalable and cost-effective Customizable nanosheet properties	Limited size/thickness control Potential defects from sonication Requires solvent removal
Supercritical CO_2-assisted exfoliation	Suitable for amorphous nanosheets Environmentally friendly	Requires specialized equipment, increasing cost and complexity Not suitable for all 2D materials

Kuriakose *et al.* introduced the liquid-phase exfoliation process for 2D MoO_3 nanosheets[21]. High-purity MoO_3 powder was initially mixed and ground with acetonitrile. The resulting mixture was then dispersed in an equal volume of ethanol and deionized water. This dispersion was subjected to ultrasonication in an ice bath for 2 h, followed by high-speed centrifugation. The supernatant was collected for subsequent device fabrication. This process not only achieved the uniform dispersion of MoO_3 nanosheets but also enabled customization of the nanosheet properties by adjusting the concentration of MoO_3 in the solution according to specific application requirements.

The liquid-phase exfoliation method is cost-effective and suitable for large-scale production. However, traditional liquid-phase exfoliation techniques still have certain limitations, and practical applications require overcoming challenges related to finer control over size and thickness. To address these limitations, supplementary methods are employed alongside traditional liquid-phase exfoliation. For example, Wei *et al.* synthesized 2D MoO_{3-x} nanosheets in 2023 using a microwave-assisted exfoliation technique [Figure 3A][22]. Figure 3B reveals that these nanosheets have an average thickness of approximately 2.8 nm. Atomic Force Microscopy (AFM) analysis indicated an average lateral dimension of 2 μm, resulting in an aspect ratio of about 670 [Figure 3C]. This aspect ratio surpasses that of previously reported 2D MoO_3 materials produced by other exfoliation techniques. Meng *et al.* successfully exfoliated monolayer α-MoO_3 using a liquid-phase ultrasonic irradiation method[23]. AFM confirmed the thickness of α-MoO_3 crystals (~1.48 nm), which is consistent with the previously reported thickness of monolayer α-MoO_3 (~1.4 nm). The results indicate that after ultrasonic and hydrothermal treatments, the van der Waals forces between MoO_3 layers were disrupted, leading to the successful production of monolayer MoO_3.

Two-dimensional amorphous materials possess unique mechanical properties, and their electrical and optical properties differ from those of crystalline materials. Supercritical CO_2-assisted exfoliation can produce 2D amorphous nanosheets, leveraging the special properties of CO_2 under supercritical conditions. When carbon dioxide is pressurized and heated beyond its critical point, it exhibits both the good diffusivity of gas and the high solvency of liquid. For example, Wu *et al.* used SC-CO_2 to prepare amorphous MoO_3 nanosheets. The amorphous structure of am-MoO_3 was confirmed by a series of characterization methods[24].

Bottom-up strategies

Bottom-up strategies for synthesizing 2D materials involve constructing these materials from the atomic or molecular level, ultimately forming macroscopic films or nanostructures. Typically, these methods can be divided into liquid-phase and vapor-phase approaches.

Hydrothermal method

Hydrothermal synthesis is a commonly used method for preparing MoO_3 nanostructures with specific morphologies by controlling the synthesis conditions. This approach is favored for its simplicity, low cost,

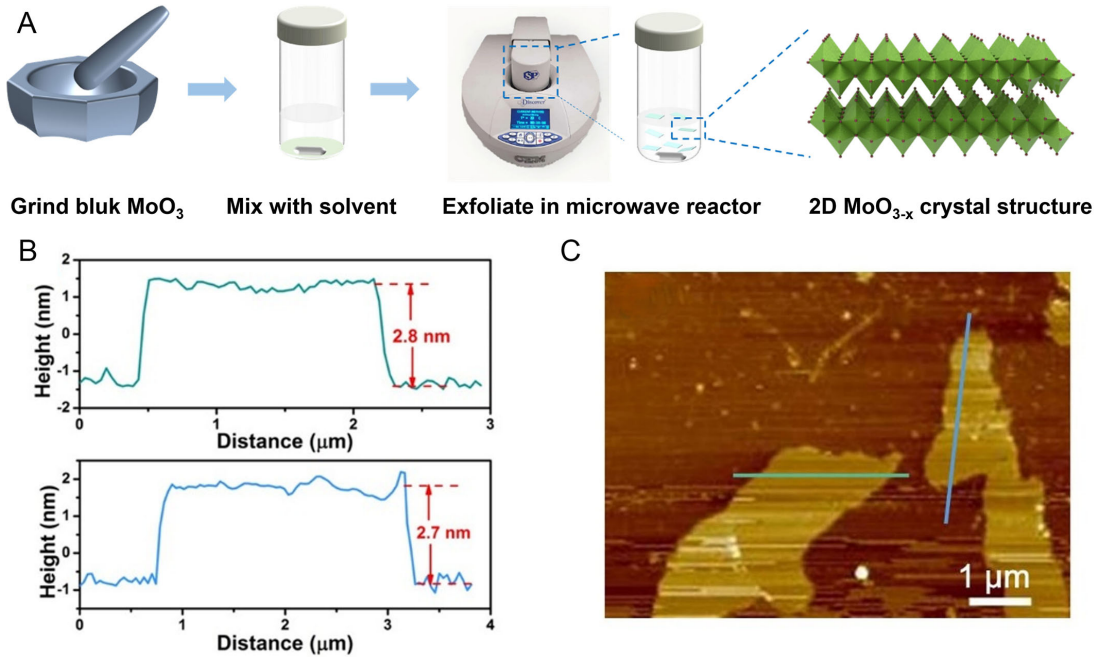

Figure 3. (A) Synthesis of MoO_{3-x} via microwave-assisted exfoliation technique. (B) Thickness measurement of exfoliated 2D MoO_{3-x} nanosheets. (C) AFM image of 2D MoO_{3-x} nanosheets. All panels reprinted with permission[22]. Copyright 2023, Elsevier.

and suitability for the fabrication of composite materials. However, because the process takes place under high-temperature and high-pressure conditions, factors such as temperature, pressure, pH, and reaction time are critical in determining the final product. Even minor variations can lead to changes in the size and morphology of the product, posing a challenge to the precise control of the dimensions of 2D materials.

The general process for the hydrothermal synthesis of 2D MoO_3 involves the following steps: Initially, a Mo precursor is dissolved in deionized water. An appropriate acid is then added, and the mixture is stirred. Subsequently, the solution is transferred to a stainless-steel autoclave reactor lined with Teflon and subjected to a hydrothermal reaction in a high-temperature oven. The resulting white powder is filtered using deionized water and ethanol, and then dried at a specified temperature. Depending on the desired control strategy and application, additional post-processing steps beyond thermal annealing can be employed, such as chemical reduction or ion exchange, to further refine the structural properties of the 2D materials. Research on the hydrothermal synthesis of 2D MoO_3 has utilized different precursors, such as $Na_2MoO_4{\cdot}2H_2O$[25], $(NH_4)_6Mo_7O_{24}{\cdot}4H_2O$[26,27], and Mo powder[28], all of which have resulted in 2D nanosheet structures of MoO_3. Additionally, Xiao *et al.* successfully obtained porous MoO_3 nanosheets with a thickness of approximately 5.5 nm and pore sizes ranging from 2 to 10 nm by controlling the annealing temperature[29].

Physical vapor deposition

Physical vapor deposition (PVD) is a technique used to deposit thin films onto substrates. This process typically involves heating a material to its evaporation point, enabling the evaporated atoms or molecules to deposit onto the substrate under vacuum or controlled atmosphere conditions. PVD technology is widely used in industrial and research applications for its ability to produce high-quality films, including in semiconductor manufacturing, optical coatings, tool coatings, and the preparation of 2D materials.

Thermal evaporation is one of the simplest PVD techniques, involving heating the raw material above its melting point until it evaporates, and then depositing it onto a cooled substrate. Although relatively simple, thermal evaporation lacks the precision needed to obtain single-layer or few-layer 2D materials.

Electron beam evaporation (EBE) uses an electron beam to heat and vaporize the material, providing higher evaporation temperatures and better control over the evaporation rate compared to thermal evaporation. Consequently, this method allows for more precise deposition of thin films. For example, Madani *et al.* used EBE to deposit MoO_x films of different thicknesses (5 and 10 nm) on glass substrates[30].

Molecular beam epitaxy (MBE) provides a highly precise and controllable methodology for the fabrication of high-quality monolayer and few-layer α-MoO_3 thin films. This technique facilitates the accurate deposition of materials through molecular beams under ultra-high vacuum (UHV) conditions, yielding superior-quality 2D films that are especially well-suited for the preparation of ultrathin films in microelectronic devices. Through MBE growth on $SrTiO_3$ (001) substrates, Du *et al.* successfully achieved self-limiting growth of monolayer α-MoO_3 thin films[31].

Pulsed laser deposition (PLD) is an advanced thin-film deposition technique that employs high-energy laser pulses to irradiate a target material, resulting in its instant vaporization and the formation of a plasma. Particles from this plasma then deposit onto a substrate to form a thin film. Due to the high energy involved and rapid cooling during the deposition process, high-quality films with superior crystallinity and uniformity can be obtained. Bisht *et al.* used PLD technology to synthesize α-MoO_3 2D layers and films[32]. Another widely used PVD technique is magnetron sputtering, which utilizes a magnetic field to enhance the electron density in the plasma, thereby increasing the sputtering efficiency and deposition rate. Zhao *et al.* used magnetron sputtering to deposit Ag and MoO_3 on a polystyrene (PS) array, forming Ag/MoO_3@PS composite materials[33].

Hot plasma-assisted techniques represent an innovative, efficient, and environmentally sustainable method for synthesizing nanomaterials. Rahman *et al.* used a cascaded arc plasma jet to generate a high-density flowing plasma stream, which interacted with a Mo metal target to synthesize 2D MoO_3 films[34]. The device is shown in Figure 4. This method not only achieves high yields but also ensures dimensional uniformity of the 2D materials, offering new possibilities for the preparation of 2D materials using physical vapor deposition techniques.

Chemical vapor deposition

Chemical vapor deposition (CVD) is a technique used for preparing high-purity, high-performance semiconductor material films. In the field of 2D materials, CVD has become one of the critical methods for fabricating large-area, high-quality 2D materials. During the CVD process, reactant gases are introduced into a high-temperature reaction chamber. These gases undergo chemical reactions or decomposition on the substrate surface, depositing to form the desired solid film. Although CVD shows great potential in the preparation of 2D materials, there remain several challenges, such as controlling the crystal phase, size uniformity, and defect density, as well as efficiently transferring the grown films to different substrates without compromising their properties. Additionally, this method imposes stringent requirements on the substrate, making it difficult for the target product to grow on substrates that do not match its lattice.

Hong *et al.* achieved controllable synthesis of ultrathin α-MoO_3 single crystals using a combination of CVD and plasma pre-treatment assistance[35]. AFM images show that the grown material has a thickness of approximately 3 nm, equivalent to about two layers of MoO_3 nanosheets. Deng *et al.* reported a flux growth

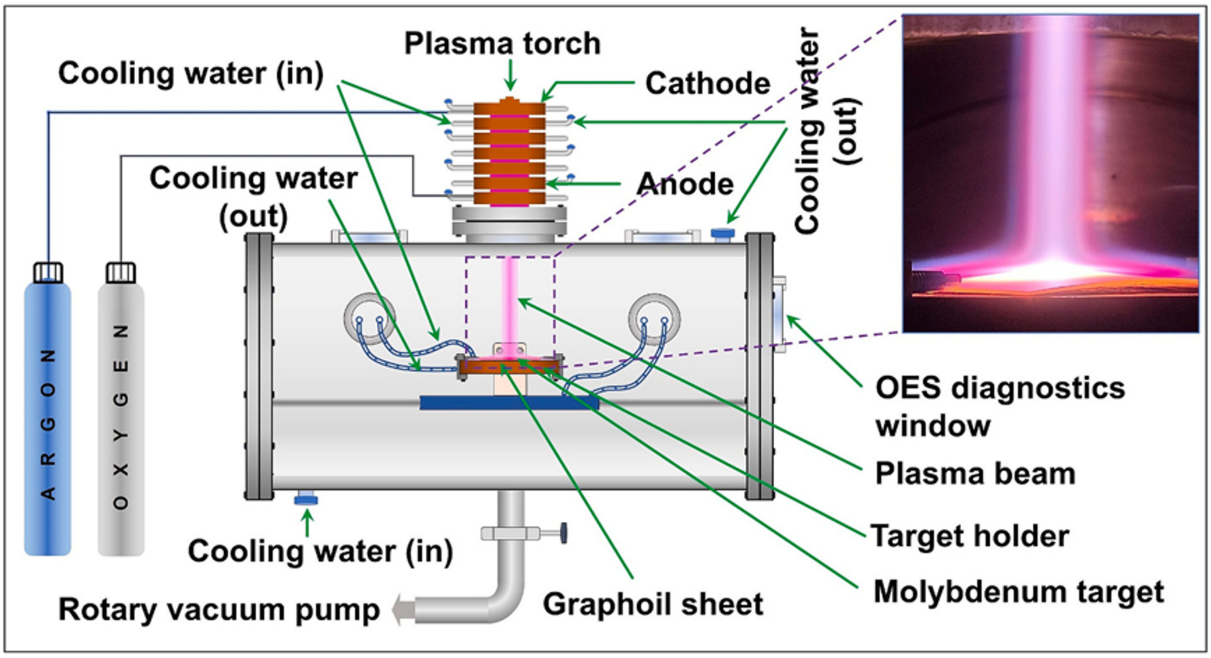

Figure 4. The plasma assisted novel experimental reactor configuration for synthesis of molybdenum-oxide nanomaterials. Inset shows that the laminar plasma beam engulfs the large molybdenum target plate, leading to high-rate generation of the metal-oxide powders (reprinted with permission[34]. Copyright 2024, Elsevier).

strategy using KCl as a flux agent to prepare 2D non-layered MoO_2 via the CVD method[36]. This approach shares similarities with the "molten salt assisted method" (MSAM) previously reported in the literature for the preparation of large-area 2D materials. By controlling the reaction temperature, homogenization time, and cooling rate, they successfully synthesized high-crystallinity non-layered 2D MoO_2 nanosheets with lateral dimensions reaching sub-millimeter scales (~464 micrometers), which represent the largest known non-layered 2D metal oxide single crystals to date [Figure 5A][36].

Atomic layer deposition (ALD), based on self-limiting surface reactions, provides an effective method for preparing MoO_3 thin films with complex optoelectronic device functionalities. Xu *et al.* used $C_{12}H_{30}N_4Mo$ as the Mo precursor and O_2 plasma as the oxygen source to deposit MoO_3 films of varying thicknesses on gold electrodes using ALD technology[37]. Kim *et al.* used ALD technology to deposit MoO_x films at 170 °C, utilizing $Mo(CO)_6$ and ozone as the Mo precursor and reactant, respectively[38]. Through rapid annealing treatment at different temperatures, they achieved the formation of self-isolated electrodes of conductive MoO_3 on TiN surfaces and insulating MoO_3 on SiO_2 surfaces.

Vapor phase epitaxy (VPE) is a specialized form of CVD known for its fast growth rates and the alignment of crystal orientation with the substrate. Lee *et al.* used the VPE method to obtain high crystalline MoO_3 nanosheets[39].

Other methods

In addition to the aforementioned methods, several alternative strategies for the preparation of 2D Mo-based oxides have been reported in the literature.

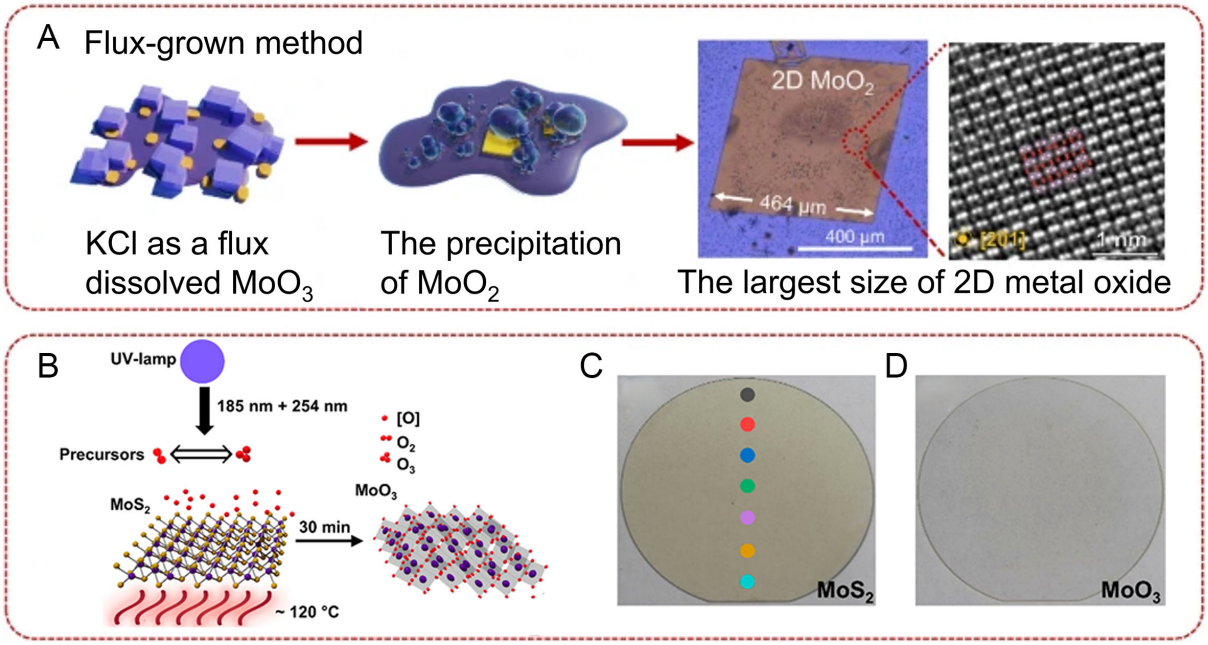

Figure 5. (A) Flux-grown method, typical SEM image of flux-grown MoO_2 flake and HAADF image of MoO_2 flake viewed along [201] zone axis. (B) UV-ozone oxidation of wafer-scale MoS_2. Under the UV light, ambient oxygen converts into ozone (ozone generation) and the generated ozone reverts (ozone decomposition) to ambient oxygen. Atomic oxygen is produced during ozone generation and decomposition, which reacts with MoS_2 and converts it to MoO_3. Two-inch sapphire wafer with MOCVD grown monolayer MoS_2 (C) before and (D) after 30 min of UV-ozone oxidation at 120 °C. The 2D MoS_2 converts into a transparent film after oxidation. (A) reprinted with permission[36],2024, CC BY license. (B-D) reprinted with permission[42].Copyright 2022, American Chemical Society.

Kundu *et al.* employed a modified co-precipitation technique, in which they adjusted the synthesis temperature and introduced a surfactant (PEG 6000) to control the phase and morphology of MoO_3[40]. They successfully synthesized 2D MoO_3 nanostructures with high specific surface area and porosity.

Zhu *et al.* used C_3N_4 as a sacrificial soft template to prepare MoO_3 nanosheets via high-temperature thermal treatment[41]. This approach avoids the use of strong acids for template removal, thereby mitigating environmental pollution.

As shown in Figure 5B, Alam *et al.* prepared wafer-scale amorphous MoO_3 monolayers through ultraviolet (UV)-ozone oxidation of MoS_2 [Figure 5C], achieving high uniformity and stability [Figure 5D][42]. Liu *et al.* utilized a simple photoradiation method to prepare MoO_{3-x} nanosheets with a layered structure[43]. Using a tungsten iodide lamp filament as the light source, they placed a piece of Mo foil on a glass or ceramic slide positioned centrally within a quartz tube. By controlling the temperature, the Mo foil was vaporized and oxidized into MoO_{3-x}. This method allows the nanosheets to grow in situ without any catalysts or templates, forming within approximately 2 min at around 535 °C in an air atmosphere.

Qi *et al.* used H_2MoO_4 as a precursor and oleic acid (OA) and oleylamine (OAm) as additives to prepare 2D MoO_{3-x} nanosheets via a one-step colloidal method[44]. Under the influence of OA and OAm, H_2MoO_4 undergoes a topological phase transformation, leading to the breaking of Mo-O bonds and a transition from the hexagonal phase to layered α-MoO_3, while also creating oxygen vacancies. The resulting MoO_{3-x} nanosheets had a thickness of approximately 2.01 nm.

STRUCTURAL REGULATION

Two-dimensional Mo-based oxides exhibit significant potential across various fields due to their unique structural characteristics and excellent physicochemical properties. However, they also face certain limitations, such as poor conductivity and insufficient density of active sites, which restrict their performance in practical applications. To overcome these limitations, researchers have proposed multiple strategies for structural modulation of 2D Mo-based oxides, aiming to enhance their performance by altering the structural features and expanding their application scope.

Here we summarize some of the structural modulation strategies for 2D Mo-based oxides, including traditional material engineering approaches such as phase transformation control, doping, and defect engineering. Given the unique structural characteristics of 2D Mo-based oxides, such as interlayer spacing, we also discuss special structural modulation strategies, specifically interlayer modulation and interface engineering.

Doping and defect engineering

Two-dimensional MoO_3 exhibits high dopability, which allows for the adjustment of its physical and chemical properties through the doping of various atoms or molecules. For example, Shkir *et al.* investigated the effects of doping rare earth elements such as Er, Gd, and Pr on the performance of MoO_3 thin films[45]. Doping led to structural changes within the MoO_3 lattice. These changes may introduce additional defects, increasing the number of adsorption sites, thereby enhancing the gas-sensing performance of MoO_3.

Non-metallic elements are also popular choices for doping. Li *et al.* found that by introducing hydrogen, 2D MoO_3 nanodisks exhibit tunable plasmonic resonance characteristics, enhancing the interaction between light and matter[46]. H-doped MoO_3 demonstrates enhanced surface plasmon resonance response in the visible to near-infrared wavelength range, thereby improving the potential application of the material in optical sensing. Furthermore, Li *et al.* proposed a method for inducing the synthesis of MoO_3 nanosheets through sulfur doping (S-doping)[47]. By adjusting the amount of S used in the solvothermal process, they prepared MoO_3 nanosheets with different morphologies. The S-doped MoO_3 nanosheets exhibited high responsiveness and selectivity towards ethanol and isopropanol[47].

For 2D metal oxides, oxygen vacancies are a critically important type of defect. By precisely controlling oxygen vacancies, the functional properties of the material can be significantly improved. In oxygen-deficient molybdenum oxides such as MoO_{3-x} ($2 < x < 3$), the presence of oxygen vacancies increases the free charge carrier density. Under illumination, the free electrons on the surface resonate collectively with incident light, leading to strong photon absorption, a phenomenon known as LSPR[48]. MoO_{3-x} exhibits a broad LSPR range (600 to 2,500 nm), and the intensity and range of LSPR can be modulated by changing the concentration of oxygen vacancies. More importantly, oxygen vacancies can act as active sites. Therefore, molybdenum oxides with controlled oxygen defects have garnered significant attention for their superior performance in electrochromic, photothermal, sensor, and catalytic applications. Sub-stoichiometric Mo-based oxides can exhibit various properties due to differing levels of oxygen vacancy content. As a result, strategies for regulating oxygen vacancy defects have received extensive research interest.

The hydrothermal method can introduce abundant oxygen vacancies during the preparation process without requiring additional steps. Li *et al.* used the hydrothermal method to prepare MoO_{3-x} nanosheets rich in oxygen vacancies and doped them with Ru elements, successfully producing Ru/MoO_{2-x} catalysts[49].

Figure 6A illustrates that the Mo^{5+} ion is in a low oxidation state, indicative of the formation of MoO_{3-x} with oxygen vacancies. Furthermore, as depicted in Figure 6B, the MoO_{3-x} phase exhibits a blue color, which transitions to white MoO_3 upon annealing in air, corroborating the presence of oxygen vacancies[50,51]. The ζ potential measurement in Figure 6C reveals a negative surface charge for MoO_{3-x} in deionized water, suggesting that the high concentration of oxygen vacancies endows MoO_{3-x} with a significant negative charge, thereby offering ample anchoring sites for Ru^{3+} adsorption. The X-ray diffraction (XRD) pattern in Figure 6D confirms the crystal structure of Ru/MoO_{2-x}. In contrast, the absence of Ru^{3+} leads to the A-MoO_{3-x} sample annealing into the MoO_3 phase (PDF#01-0706), rather than the MoO_2 phase, indicating the structural transition induced by Ru incorporation. Figure 6E and F shows that Ru/MoO_{2-x} retains the nanolayered structure of the MoO_{3-x} precursor, with Ru nanoclusters visible within the red box in the high-resolution transmission electron microscopy (HRTEM) image [Figure 6G]. The annular dark field scanning transmission electron microscopy (ADF-STEM) image displays lattice fringes with a spacing of 0.208 nm, corresponding to the (101) plane of Ru [Figure 6H and I]. Consequently, the presence of oxygen vacancies facilitates the anchoring of Ru^{3+}, and the addition of Ru promotes the formation of Ru-O-Mo sites, thereby enhancing the conversion of MoO_3 to MoO_2. Research by Sun *et al.* demonstrated that by adjusting the temperature and the ratio of ethanol to deionized water during the hydrothermal synthesis process, the concentration of oxygen vacancies can be effectively controlled[52]. They fabricated MoO_{3-x}-based H_2S sensors and found that the MoO_{3-x} material with the highest concentration of oxygen vacancies exhibited the best detection performance for H_2S.

In addition, Sun *et al.* reported a strategy utilizing a rapid carbon thermal shock method to construct oxygen vacancies on MoO_2 and prepare Fe-MoO_2 electrocatalysts[53]. In this strategy, rapid carbon thermal shock was used to introduce Fe atoms into MoO_2. Due to the different spin states of Fe and Mo, the introduction of Fe atoms leads to abundant lattice misalignments in Fe-MoO_2, promoting the formation of oxygen vacancies. During the rapid heating and cooling process, extreme temperature changes cause lattice distortion and stress, further facilitating the formation of oxygen vacancies. The incorporation of Fe atoms and the abundance of oxygen vacancies in MoO_2 can alter the distance of Mo-O bonds, modulate the electronic structure, and optimize the performance of the catalyst[53].

Studies have shown that combining doping and defect engineering strategies can yield better results. Xu *et al.* used Ce-ion-doped oxygen-vacancy MoO_3 ultrathin nanosheets as the anode material for asymmetric supercapacitors[54]. In their study, Mo powder was used as the precursor, and under the preferential growth mechanism induced by Ce doping, the construction and thickness control of ultrathin oxygen-vacancy Ce-doped MoO_3 nanosheets were achieved. The optimized Ce-doped OV-MoO_3 exhibited very high specific capacitance and demonstrated long-term stability.

Interface engineering

Interface engineering involves the design and control of the chemical and physical properties at the interfaces between materials. Heterojunctions have been a popular topic in the study of interface engineering for 2D materials. By stacking different types of 2D semiconductor materials, artificial heterojunction structures can be created. These structures can give rise to new physical phenomena and can be designed to have specific functionalities for devices. Due to the single-layer nature of 2D materials, their interactions can be achieved through van der Waals forces, eliminating the need for precise lattice matching required in traditional semiconductors.

Ou *et al.* employed a simple probe sonication method to synthesize Dy_2O_3/MoO_3 2D heterostructures, which enable high sensitivity ammonia detection at lower temperatures[25]. Figure 7A-C shows the energy

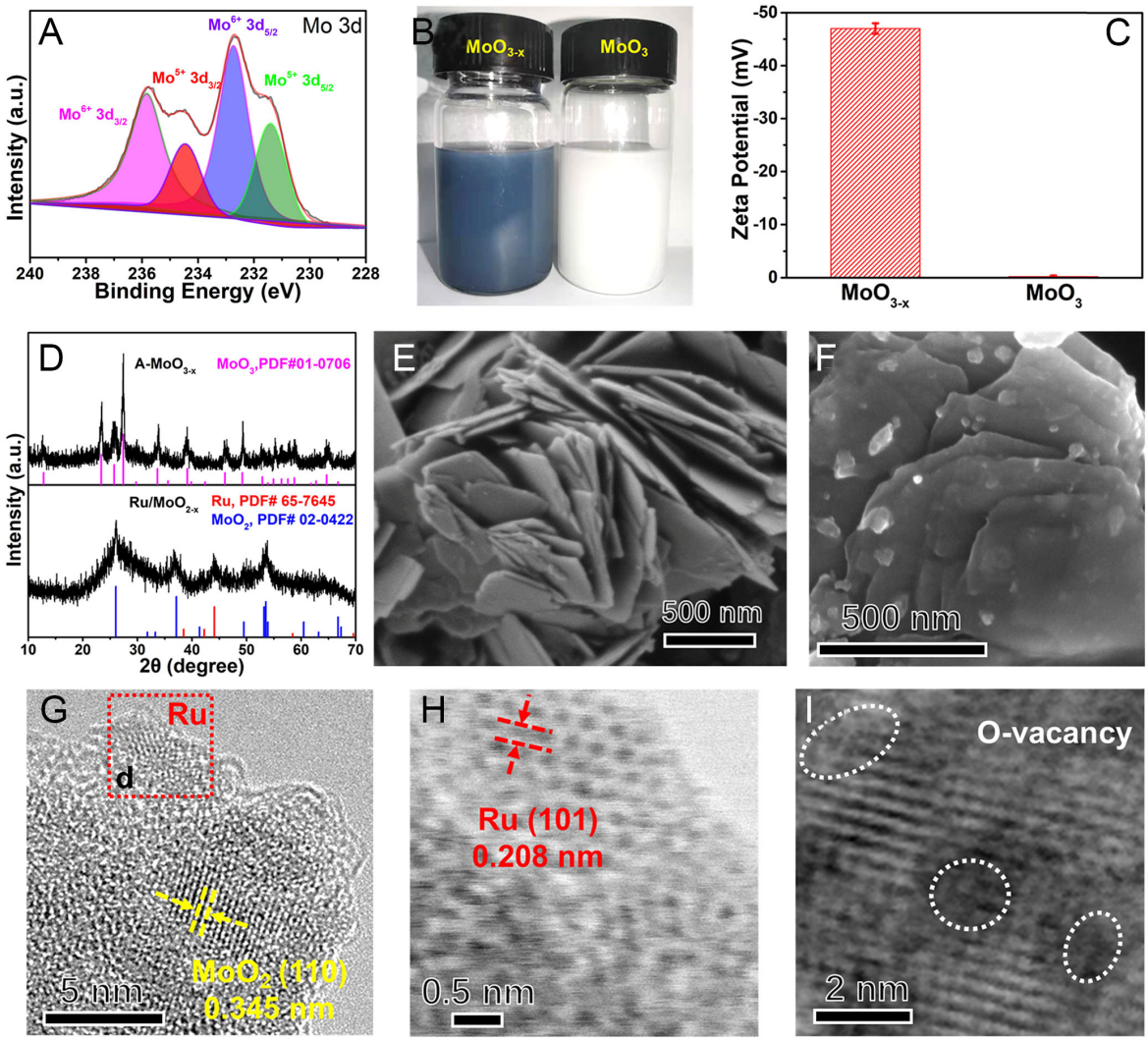

Figure 6. (A) Mo 3d core level spectrum. (B) The photographs of the MoO_{3-x} and MoO_3 powder dispersed in ethanol. (C) Comparison of zeta potential of MoO_{3-x} and MoO_3. (D) XRD pattern. (E) SEM image of MoO_{3-x}. (F) SEM, (G) HRTEM, (H and I) ADF-STEM images of Ru/MoO_{2-x}. All panels reprinted with permission[49]. Copyright 2022, Elsevier.

levels within Dy_2O_3/MoO_3 composite. The abundance of heterojunctions enhances the regulation of carrier concentration, and the compensatory/protective effect of Dy_2O_3 mitigates the impact of humidity, giving the sensor good humidity independence. Due to the difference in work functions between the two materials, electrons transfer from Dy_2O_3 to MoO_3, causing more oxygen molecules to be attracted to the MoO_3 side, which promotes NH_3 adsorption and electron release, thereby enhancing the sensor response [Figure 7D and E]. Pradeep Kumar *et al.* prepared MoS_2/MoO_3 nanocomposites, forming p-n heterojunctions within the material[26]. The formation of these heterojunctions alters the band structure, enhancing carrier transport within the device. Moreover, the heterojunction provides more adsorption sites, facilitating the adsorption of gas molecules onto the sensor surface. In the research conducted by Lin *et al.* on organic photovoltaic devices, the use of a heterojunction formed by Br-2PACz and MoO_3 not only improved the power conversion efficiency of the devices but also enhanced their operational stability under continuous illumination and heating conditions[55]. This enhancement is primarily attributed to the ability of the heterojunction to suppress the diffusion of Mo ions into the bulk heterojunction and promote a favorable distribution of donor and acceptor components.

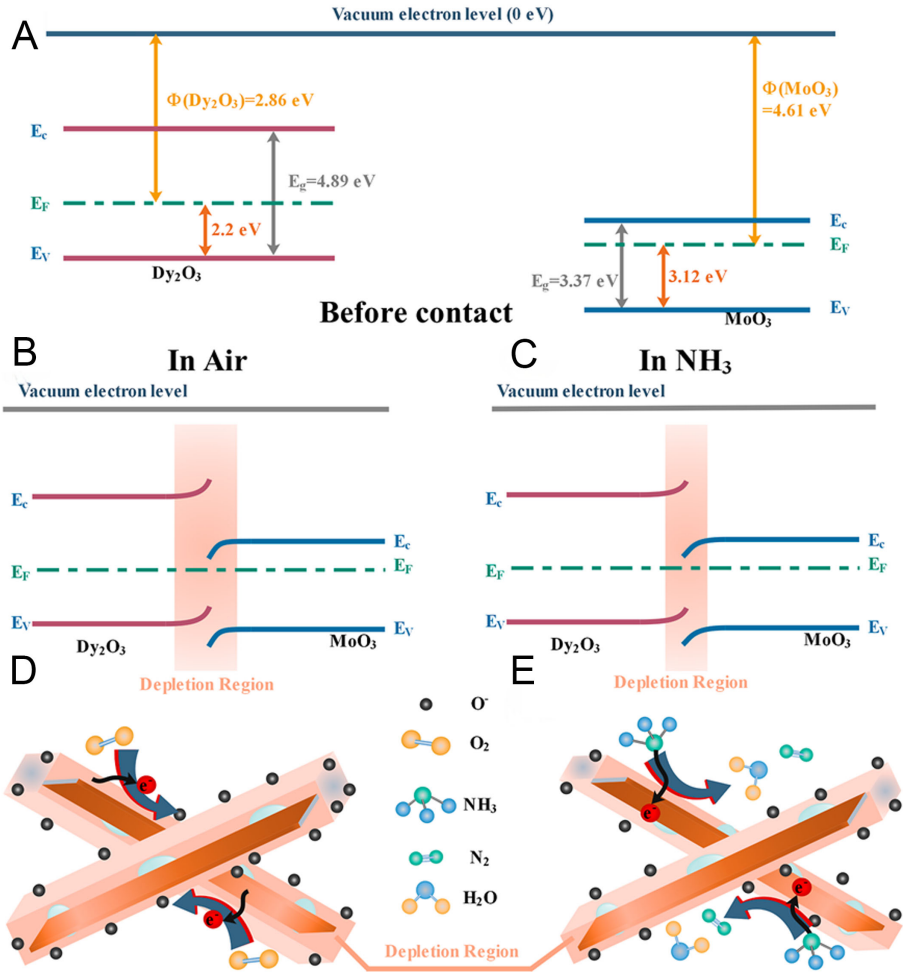

Figure 7. (A) Schematic illustration of the energy levels within Dy_2O_3/MoO_3 composites before contact and after contact, (B) In air, and (C) In NH_3 and the corresponding diagram of the gas-sensing process (D) In air and (E) In NH_3. All panels reprinted with permission[25]. Copyright 2023, American Chemical Society.

Similar to p-n junctions, Schottky junctions are another type of interface structure formed by the contact between a metal and a semiconductor. For example, Ding *et al.* prepared Mo-modified MoO_3 nanosheets using a method that enhances photocatalytic efficiency through the synergistic effect of *in-situ* constructed Schottky junctions and oxygen vacancies[28]. The Schottky barrier formed between Mo and MoO_3 creates a built-in electric field, which facilitates charge separation during the photocatalytic process. Characterization methods such as electrochemical impedance spectroscopy can further confirm that the construction of a Schottky junction is more beneficial for charge transfer and separation of photogenerated charges compared to oxygen vacancies alone.

Z-type heterojunctions exhibit several advantages over traditional heterojunctions, particularly in enhancing photocatalytic efficiency. For instance, in the Z-type heterojunction constructed by Wang *et al.* between

MoO_3 and g-C_3N_4, the conduction band position of MoO_3 is close to the valence band position of g-C_3N_4, which facilitates the migration of carriers[56]. Additionally, oxygen vacancies present in MoO_3 act as shallow donors, imparting metallic conductivity to MoO_3 and serving as new active sites, which help adjust the bandgap and promote visible light absorption and utilization. The 2D/2D Z-type heterojunction formed by MoO_3/g-C_3N_4 not only increases the density of active sites and promotes the separation of photogenerated carriers but also enhances photocatalytic activity. Furthermore, the matched energy band positions and reduced aggregation contribute to enhanced catalytic activity and stability.

Peng *et al.* synthesized 0D/2D CdS/MoO_{3-x} heterojunctions via a simple co-precipitation method[57]. The introduction of CdS nanoparticles forms an S-scheme heterojunction with MoO_{3-x}. In this heterojunction, the interface between CdS and MoO_{3-x} creates an internal electric field, which effectively separates photogenerated electrons and holes, enhancing charge separation effect. The structure of the S-scheme heterojunction also shortens the migration distance between electrons and holes, accelerating charge separation. This charge transfer mechanism [Figure 8A] helps to enhance the plasmonic resonance effect caused by the abundant oxygen vacancies in MoO_{3-x} and enables the 0D/2D CdS/MoO_{3-x} heterojunction to possess higher photocatalytic H_2 generation capability, approximately 10.3 times that of the original CdS nanoparticles [Figure 8B and C]. Similarly, Wei *et al.* synthesized a 1D/2D $Zn_{0.1}Cd_{0.9}S$/MoO_{3-x} S-scheme heterojunction by loading 1D $Zn_{0.1}Cd_{0.9}S$ nanorods onto 2D MoO_{3-x} nanosheets[58]. The charge transfer mechanism of the S-scheme heterojunction enhances the redox capabilities of the carriers, resulting in excellent photocatalytic H_2 generation rates, approximately six times higher than those of pure $Zn_{0.1}Cd_{0.9}S$. Wang *et al.* prepared a dual plasmon-enhanced 2D/2D/2D g-C_3N_4/Pd/MoO_{3-x} (CPM) S-scheme heterojunction[59]. The dual LSPR effect of MoO_{3-x} and Pd nanosheets synergistically broadens the optical response range of CPM, enhancing the photocatalytic activity.

When material type is not a limiting factor, the contact between materials can be extended to multiple layers to form heterostructures. Yoon *et al.* found that the high work function of MoO_3 can reduce the contact resistance with MoS_2, eliminating the Fermi level pinning effect[60]. This makes the MoS_2-MoO_3 heterostructure highly promising for applications as p-type transistors. Krishnan *et al.* revealed that the MoO_3-hBN heterostructure exhibits incoherent stacking due to lattice mismatch, which enables ultralow friction because they possess low shear strength in all sliding directions[61]. Compared to homo-bilayers such as MoO_3-MoO_3 or hBN-hBN, the heterostructure provides a lower coefficient of friction.

The studies presented in this section highlight the significant potential of interface engineering in enhancing the performance of 2D Mo-based oxides. A common trend across these studies is the critical role of band alignment, interfacial defects, and charge transfer dynamics in determining the performance of heterojunction-based devices. However, challenges remain in achieving precise control over interface properties, such as defect density and interfacial strain, which can significantly impact device performance.

Interlayer tuning

MoO_3 has its internal layers connected by covalent bonds and separated by van der Waals forces. When foreign substances such as metal ions or other compounds are intercalated between these layers, the interlayer spacing of MoO_3 is altered, thus influencing its physical properties. Wang *et al.* introduced a composite material prepared by inserting Keggin-type polycationic $AlO_4Al_{12}(OH)_{24}(H_2O)_{12}^{7+}$ (Al_{13}) into the interlayers of MoO_3[62]. These composites can rapidly adsorb anionic dye methyl orange (MO) through strong electrostatic interactions, leading to the formation of tight and stable aggregates around the charged Al_{13} clusters.

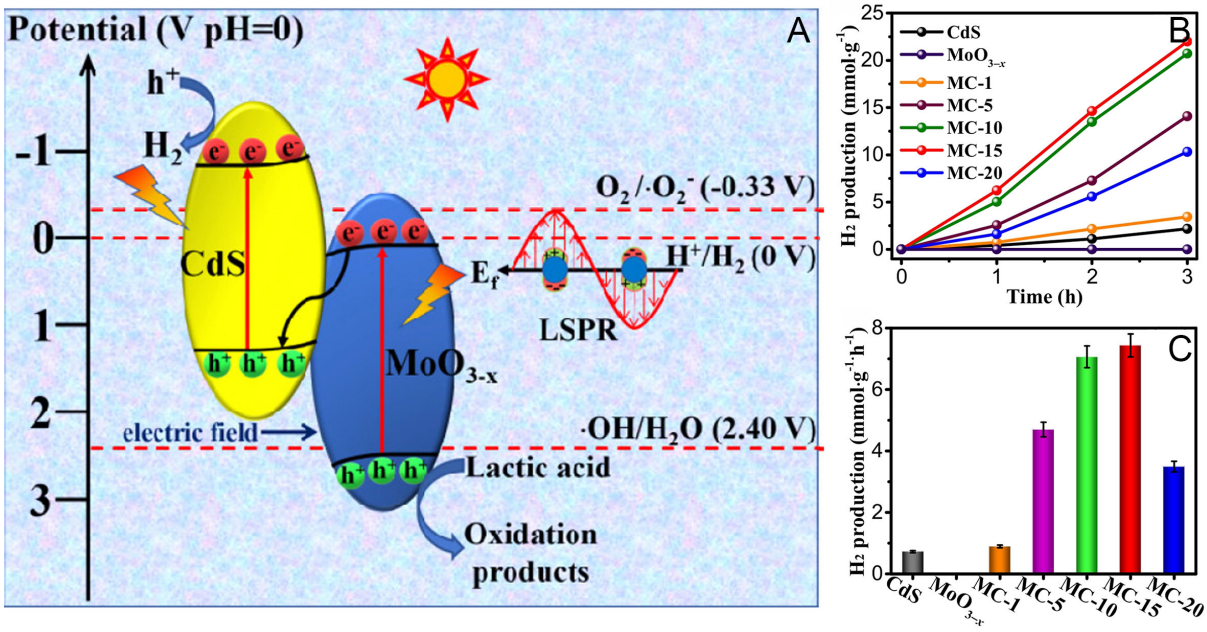

Figure 8. (A) Mechanism of photocatalytic H_2-production using CdS/MoO_{3-x} composites. Photocatalytic H_2 evolution performances (B) and H_2 evolution rates (C) of CdS, MoO_{3-x}, MC-15 is a composite material containing 15 wt% MoO_{3-x} nanosheets. All panels reprinted with permission[57]. Copyright 2021, Elsevier.

Intercalation can improve the electrochemical performance of MoO_3 when used as a cathode material, as confirmed by the research of Tan *et al.* By intercalating organic molecules such as polyaniline (PANI) into MoO_3, the storage capacity for Zn^{2+} can be effectively enhanced[63]. The insertion of PANI not only increases the interlayer spacing of MoO_3 but also stabilizes the layered structure of MoO_3, thereby improving the capacity and cycling stability of the material.

Gao *et al.* synthesized ultra-thin nanosheets of Li-ion intercalated MoO_{2-x} and prepared Fe@MoO_{2-x}/Li ultra-thin nanosheets for use as catalysts in ammonia synthesis[64]. Through thermal treatment, Li ions and electrons were intercalated into the MoO_2 layers, causing lattice expansion. The introduction of electrons reduces the oxidation state of Mo, generating MoO_{2-x}. The downshift of the d-band in MoO_{2-x} lowers the activation energy of the reaction, thus promoting ammonia synthesis. The introduction of Fe significantly facilitates the intercalation of Li ions and the exfoliation of MoO_2, further lowering the energy barrier of the reaction[64].

Reed *et al.* chose different metal intercalants (Au, Cr, Fe, Ge, Mn, and Ni) to modulate α-MoO_3[65]. The study demonstrated that the anisotropy of α-MoO_3 can be regulated by selecting different metal intercalants. Except for Ge-MoO_3, all other intercalations reduced the anisotropy of MoO_3. Additionally, the color of the materials changed from transparent white to near black or dark blue, which is associated with a reduction in the bandgap and increased absorption at wavelengths greater than 600 nm, particularly for Cr-, Ge-, and Mn-MoO_3 intercalated samples.

Hu *et al.* reported a strategy for preparing organic/inorganic superlattice structures through organic intercalation[66]. By co-intercalating Na^+/H_2O into MoO_3 nanoribbons and then performing guest exchange in situ polymerization with aniline monomers, they obtained 2D PANI/MoO_{3-x} superlattice nanosheets. The embedding of PANI not only induces the structural morphological transformation of MoO_3 nanoribbons

into 2D PANI/ MoO_{3-x} superlattice nanosheets but also partially reduces Mo^{6+} to Mo^{5+}, creating abundant oxygen vacancies. Consequently, the 2D PANI/MoO_{3-x} superlattice nanosheets exhibit excellent Fenton-like catalytic activity in the generation of ·OH from H_2O_2.

Interlayer tuning represents a versatile strategy for modulating the properties of 2D Mo-based oxides. However, achieving precise control over the intercalation process remains challenging, particularly with respect to uniformity and scalability. Future research should focus on exploring novel intercalants with multifunctional properties, such as those capable of simultaneously enhancing conductivity and catalytic activity. The development of large-scale intercalation methods will also be critical for the practical application of these materials in energy storage and catalysis. By addressing these challenges, interlayer tuning can continue to unlock new possibilities for the design and optimization of 2D Mo-based oxides.

Phase transition

Phase transitions, as a common regulation strategy, have been extensively studied in the field of materials science. For 2D transition metal oxides such as MoO_3, phase transitions can bring about unique physical properties, such as enhanced electrochemical performance, improved optical characteristics, and mechanical properties. By applying different external conditions to the material, such as pressure or temperature changes, a phase transition can be induced, altering the crystal structure, bandgap width, and optical absorption properties. Under high pressure, MoO_3 undergoes significant structural changes. At around 11 GPa, the orthorhombic α-MoO_3 (Pnma) phase transforms into the monoclinic MoO_3-II phase ($P2_1/m$). This transition is driven by shear stress, which causes a rearrangement of the MoO_6 octahedra and a change in the stacking sequence of the layers, leading to the loss of the original 2D layered structure. As the pressure increases further to around 27 GPa, MoO_3-II undergoes another phase transition to form the orthorhombic MoO_3-III phase (Pmma). This transition is marked by the disappearance of out-of-plane vibrational modes, indicating the complete loss of the layered structure and the formation of a 3D crystalline phase[67]. These high-pressure phases exhibit distinct optical and electronic properties, such as a narrower bandgap and enhanced optical absorption, which are crucial for potential applications in optoelectronics and energy storage.

Wang *et al.* focused on the effects of high pressure on the phase transitions of MoO_3 and the changes in its optical properties[68]. They found that under a pressure of 10 GPa, the α-phase MoO_3 transforms into another high-pressure phase, MoO_3-II. When the pressure exceeds 25 GPa, it transforms into MoO_3-III. After releasing the pressure, the MoO_3-II phase remains stable, indicating that the phase transition is irreversible. In terms of optical properties, the quenched MoO_3-II phase exhibits a narrower bandgap (reduced by approximately 25%) and stronger optical absorption within the bandgap compared to the original low-pressure α-MoO_3 phase. This discovery is significant for exploring high-pressure phase materials for applications under ambient pressure conditions.

The work by Kundu *et al.* involves using an improved co-precipitation method to prepare MoO_3 nanostructures[40]. Through a simple surfactant-assisted synthesis process and slight temperature variations, researchers successfully achieved a phase transition from hexagonal phase MoO_3 nanorods to α-MoO_3 nanosheets. These 2D α-MoO_3 nanosheets exhibited superior electrochemical performance, attributed to their larger specific surface area and the presence of open van der Waals gaps. Particularly when used as electrode materials for asymmetric all-solid-state supercapacitors, they showed a high pseudocapacitive response. Additionally, these materials retained up to 91% of their initial specific capacitance after 2,000 charge-discharge cycles at a current density of 5 A g^{-1}, demonstrating excellent electrochemical stability.

APPLICATIONS

This section will focus on the recent applications of 2D Mo-based oxides in various fields, including energy and catalysis, sensors, and electronic and optoelectronic devices. While some studies have previously discussed synthesis methods and tuning strategies, this section will primarily emphasize the performance of these materials. Table 2 summarizes the applications of 2D Mo-based oxides in recent years.

Energy and catalysis

The superior performance of 2D materials in energy-related applications is attributed to their atomic-scale thickness and unique physical properties, including high surface area and tunable electronic properties. These features enable higher density of active sites and controllable catalytic properties, rendering them highly adaptable for various energy technologies[69]. Moreover, their mechanical flexibility, optical transparency, and superior thermal conductivity further enhance their applicability in fields ranging from energy storage to conversion and harvesting.

Supercapacitors and batteries

Two-dimensional materials such as graphene exhibit high specific surface area, excellent electrical conductivity, and chemical stability, qualifying them as ideal electrode materials for supercapacitors. The capacitive performance of these materials can be further enhanced by manipulating their layer count or through integration with other materials.

Two-dimensional MoO_3, with its multiple possible oxidation states, can engage in numerous REDOX reactions during the charge-discharge cycle, thereby broadening the electrochemical window. Additionally, MoO_3 is cost-effective, eco-friendly, and boasts a high theoretical capacity (1,005 C g^{-1}). Notably, α-MoO_3 has been the subject of extensive research due to its anisotropic layered structure, which aids in the intercalation and deintercalation of electrolyte ions. Nevertheless, MoO_3 faces challenges such as its low electrical conductivity, which affects its current response and capacitance characteristics. To enhance its performance, it is imperative to optimize crystal size and morphology[40]. Zhu *et al.* enhanced the properties of MoO_3 nanosheets using a templating method, achieving a specific capacitance of up to 994.2 F g^{-1} in an acidic electrolyte at a current density of 0.5 A g^{-1}[41]. A supercapacitor device constructed with YP50 as the negative electrode and MoO_3 as the positive electrode reached an energy density of 35.5 Wh kg^{-1}. Moreover, the device operated at a power density of 350.0 W kg^{-1} and maintained 84% of its initial specific capacitance after 1500 cycles, demonstrating commendable cycle stability.

In lithium-ion batteries and beyond, 2D MoO_3 serves as an electrode material, offering enhanced capacity and rapid charging capabilities. Moreover, it can be employed as a separator coating to bolster the safety and cycle stability of batteries. Studies have shown that MoO_3 can modify lithium-sulfur battery separators, enhancing their initial capacity and cycle stability[70]. Hsu *et al.* introduced α-MoO_3 as a material for Al-ion energy storage within an air-stabilized hydrated eutectic electrolyte (ASHEE) system[71]. The α-MoO_3 electrode exhibits a high capacity of approximately 285 mA h g^{-1} and maintains about 86% of its capacity after 40 charge-discharge cycles at a current density of 0.4 A g^{-1}. These findings suggest that α-MoO_3 holds promise as a positive electrode material for Al-ion storage in ASHEE systems.

Photocatalysis

In photocatalysis, 2D MoO_3 absorbs specific light wavelengths and generates electron-hole pairs due to its unique band structure, facilitating chemical reactions. Introducing oxygen vacancies or forming heterojunctions can significantly enhance the catalyst's performance, thereby increasing the efficiency of the target reaction. Photocatalysis, encompassing applications such as pollutant degradation, H_2 production,

Table 2. Summary of recent 2D Molybdenum oxide applications

Applications		Materials	Performance metrics	Refs.
Energy and catalysis	Supercapacitors and batteries	MoO_3	Specific capacitance: 994.2 F g^{-1} at 0.5 A g^{-1} Energy density: 35.5 Wh kg^{-1}	[41]
		α-MoO_3	Capacity: 285 mA h g^{-1} at 0.4 A g^{-1} Capacity retention: 86% after 40 cycles	[71]
	Photocatalysis	MoO_3@ZrO_2	DS removal rate: 90.94%	[73]
		Cu-α-Fe_2O_3/α-MoO_3	NPOC removal rate: 76.29%	[74]
		Ce-MoO_3	Photocatalytic activity: 2,858 mA mg^{-1}	[75]
		MoO_3/g-C_3N_4	H_2 generation rate: 328.75 μmol·g^{-1}·h^{-1}	[56]
		Mo@MoO_3	NH_3 production rate: 50.78 μmol·g^{-1}·h^{-1}	[28]
		cellulose over MoO_3	NH_3 production rate: 68 μmol·h^{-1}·g^{-1}	[27]
	Electrocatalysis	Ru/MoO_{2-x}	Overpotential: 29 mV at 10 mA cm^{-2} Tafel slope: 22 mV dec^{-1}	[49]
		P- Fe_3O_4-MoO_2	Overpotential: 189 mV at 10 mA cm^{-2}	[77]
		Pd@MoO_3	Overpotential: 71 mV at 10 mA cm^{-2} Tafel slope: 42.8 mV dec^{-1}	[78]
		am-MoO_3	NH_3 production rate: 480.4 μmol·cm^{-2}·h^{-1} Faraday efficiency: 94.8%	[24]
	Solar cells	L-MoO_x	PCE: 22%	[80]
		SnS/MoO_3	PCE: 4.4%; V_{OC}: 437 mV	[81]
		US-MoO_x	PCE: 19.6%	[82]
Sensors		a-MoO_3	Limit of detection for o-AAT: 10^{-9} M	[23]
		Dy_2O_3/MoO_3	10 ppm NH_3 response: 30.52 at 328.2 °C;	[25]
		MoO_3	10 ppm DIPA response: 30.4 at 217 °C;	[29]
		MoO_3	Humidity sensitivity: 9,794 Ω/RH at 25 °C	[84]
Electrochromism		W-doped MoO_3	Switching time: 3.9 s coloring efficiency: 40.43 cm^2 C^{-1}	[86]
		MoO_3	N/A	[21]
Electronic and optoelectronic devices		MoO_3	OTFT-Ag/MoO_3/NPB on/off ratio: 3.72 × 10^3	[88]
		α-MoO_3	Memristor response: 10 μs R_{off}/R_{on}: > 10^4	[89]
		α-MoO_3	Set voltage: 0.5 V; on/off ratio: 10^4	[35]
		MoO_3	Threshold switching voltage: +0.73 V; Applied current: 4-6 × 10^{-7} A	[37]
		$CsPbBr_3$ QDs/MoO_3	Photodetector responsivity: 8.4 A/W in UV light; on/off ratio: 118	[39]

CO_2 reduction, and N_2 fixation, represents a promising approach to realizing green, efficient, and safe technologies[72].

Ashraf *et al.* synthesized a novel MoO_3@ZrO_2 nanocomposite with a Z-type heterostructure for the degradation of diclofenac sodium (DS)[73]. This nanocomposite achieved a DS removal rate of 90.94% under simulated light/peroxymonosuifate (PMS) conditions, demonstrating high stability and recyclability. This study underscores the significant potential of MoO_3@ZrO_2 composites for innovative water purification solutions powered by visible light. Wang *et al.* developed a hydrothermal oxygen decoupling (HTOU) system using a Cu-α-Fe_2O_3/α-MoO_3 catalyst for biogas sludge (BS) treatment[74]. This catalyst exhibits van der Waals heterojunction and REDOX properties. Experimental results indicate that the Cu-α-Fe_2O_3/α-MoO_3 catalyst achieved removal efficiencies of 76.29% for non-volatile organic carbon (NPOC), 45.56% for total nitrogen (TN), and 29.03% for ammonia nitrogen (AN) after 30 min reaction at 225 °C. The significant

deactivation of the catalyst was attributed to aromatic polymer deposition and heavy metal contamination. This research highlights the potential of efficient and cost-effective oxygen decoupling to enhance hydrothermal treatment of highly concentrated organic wastewater.

Zhao *et al.* synthesized a Ce-MoO_3 nanosheet-supported Pt nanoparticle catalyst with oxygen vacancies (OVs-Ce-MoO_3/Pt), demonstrating exceptional performance in electrocatalysis and photocatalytic oxidation of methanol[75]. The catalyst exhibited a photocatalytic activity of 2,858 mA mg^{-1}, surpassing other catalysts in terms of anti-poisoning ability and long-term stability[75].

Wang *et al.* constructed a 2D/2D Z-type heterojunction photocatalyst, MoO_3/g-C_3N_4, with enhanced REDOX capabilities for photocatalytic hydrogen production and tetracycline (TC) degradation[56]. The 3% MoO_3/g-C_3N_4 composite achieved an optimal hydrogen generation rate of 328.75 μmol·g^{-1}·h^{-1}, approximately 87-fold higher than that of pure g-C_3N_4 without any noble metal cocatalyst. Additionally, the degradation kinetic constant for TC was 0.0196 min^{-1}, about 8.28 times that of pure g-C_3N_4.

The research by Ding *et al.* revealed that the N_2 photocatalytic nitrogen fixation performance of Mo@MoO_3 nanosheets, prepared via solvothermal synthesis, reached 50.78 μmol·g^{-1}·h^{-1}, nearly three times that of commercial MoO_3[28]. The Schottky barrier-generated internal electric field facilitates charge transfer during the photocatalytic reaction, while oxygen vacancies capture electrons to activate N_2. By combining with Mo, the MoO_3 nanosheets broadens the light absorption range and enhances the transfer of excited electrons to the active site. Wang *et al.* developed a photocatalytic system that employs MoO_3 nanosheets with oxygen vacancies as photocatalysts for the nitrogen fixation reaction [Figure 9][27]. Cellulose, a naturally abundant and renewable material, serves as a sacrificial reagent. Within this system, the photooxidation of cellulose yields value-added chemicals and supplies electrons necessary for N_2 reduction, resulting in a peak ammonia (NH_3) production rate as high as 68 μmol·h^{-1}·g^{-1}. This study offers significant insights into strategies for converting N_2 and cellulose into value-added chemicals through nitrogen fixation[27].

Electrocatalysis

Electrolysis of water or electrochemical water splitting for hydrogen production has been receiving attention due to its promising prospects, with advantages such as stable output, high purity of hydrogen, and scalability. However, due to the slow rate of the hydrogen evolution reaction (HER), there has been ongoing research into efficient electrocatalysts to accelerate this process[76].

Li *et al.* prepared a Ru/MoO_{2-x} catalyst that demonstrated exceptional performance in alkaline HER, achieving an ultra-low overpotential of 29 mV at a current density of 10 mA cm^{-2}[49]. The current density of this catalyst was 7.3 times higher than that of commercial Pt/C [Figure 10A and B], and it maintained its performance stability even after 1,000 cycles of cyclic voltammetry [Figure 10C]. This positions the Ru/MoO_{2-x} catalyst as a potential replacement for precious metal catalysts. Similarly, Wang *et al.* have demonstrated an enhancement in the electrocatalytic performance of MoO_2 by synthesizing P-doped Fe_3O_4-MoO_2 nanosheets supported on N-doped carbon flakes, thereby altering the electronic configuration of MoO_2[77]. Benefiting from the synergistic effects of P doping, the heterojunction interface, and the support provided by the N-doped carbon matrix, the synthesized P-Fe_3O_4-MoO_2/NC material displayed superior activity for water electrolysis, exhibiting notable stability and surpassing the performance of commercially available RuO_2 catalysts. In addition, Li *et al.* successfully designed a Pd@MoO_3 heterostructure by confining Pd nanoparticles and atomically dispersed Pd sites into defect-rich 2D MoO_3 nanosheets through the interface engineering strategy, significantly enhancing its HER performance in an acidic medium[78]. The catalyst exhibited outstanding HER activity, with an overpotential of 71 mV and a Tafel slope of

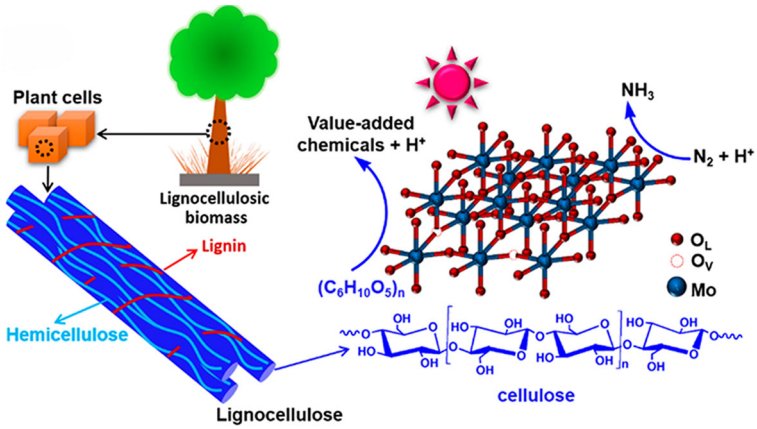

Figure 9. Schematic presentation of photocatalytic nitrogen fixation coupled with the generation of value-added chemicals from N_2 and cellulose over MoO_3 nanosheets as well as the composition and structure of cellulose in lignocellulosic biomass. Reprinted with permission[27].Copyright 2024, American Chemical Society.

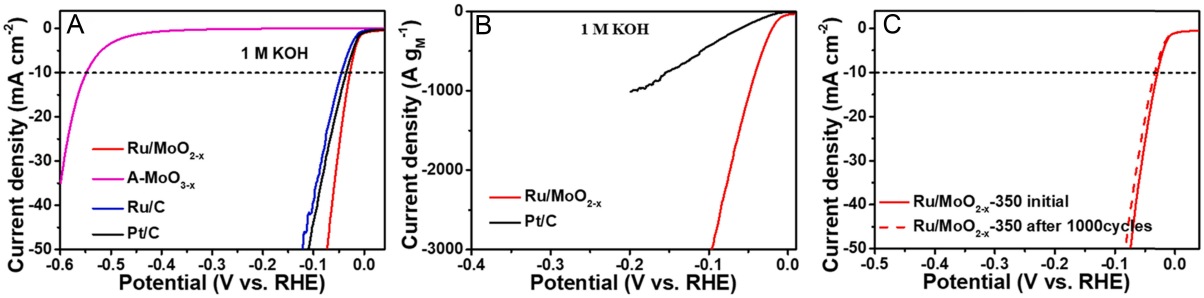

Figure 10. (A) LSV curves of Ru/MoO_{2-x}, A-MoO_{3-x}, Ru/C, and commercial Pt/C catalyst in 1 M KOH. (B) The mass activities of Ru/MoO_{2-x} and Pt/C. (C) Durability of Ru/MoO_{2-x} for 1,000 cycles CV cycles in 1 M KOH. All panels reprinted with permission[49]. Copyright 2022, Elsevier.

42.8 mV dec^{-1} in 0.5 M H_2SO_4 solution, along with excellent stability. This work provides new insights for the development of highly efficient and cost-effective catalysts.

Wu *et al.* reported on a novel, efficient, and durable catalyst for the electroreduction of nitrite ions to ammonia - amorphous MoO_3 nanosheets[24]. The am-MoO_3 catalyst achieved a maximum NH_3 yield of 480.4 μmol·cm^{-2}·h^{-1} at -0.6 V *vs.* the reversible hydrogen electrode (RHE) and exhibited a Faraday efficiency of up to 94.8% for converting NO^{2-} to NH_3. Moreover, the catalyst demonstrated excellent long-term stability, withstanding continuous electrolysis tests for up to 30 h.

Solar cells

Mo-based oxide films are commonly employed in solar cells due to their high work function and broad band gap. As a hole transport layer, they effectively facilitate hole transport and minimize contact recombination, thereby enhancing the device's efficiency and stability[79]. Li *et al.* investigated the use of low-oxygen MoO_x (L-MoO_x) films as hole transport layers to boost the efficiency and stability of crystalline silicon solar cells[80]. The L-MoO_x films, deposited using a MoO_2 evaporation source, possess a wide band gap that inhibits the diffusion of Ag and Si into MoO_x, thereby improving the device's stability in ambient conditions.

Suzuki *et al.* fabricated solar cells using n-type SnS single crystal junctions combined with MoO_3 thin films to elevate the V_{OC}. They achieved a record-high V_{OC} of 437 mV for SnS solar cells[81]. Wang *et al.* developed a series of organic photovoltaic cells with an impressive photoconversion efficiency of 19.6%[82]. In their design, a 7 nm-thick MoO_x layer was incorporated into the interconnecting layer (ICL). The MoO_x layer, integrated with materials such as Ag and ZnO:PFN-Br, formed a comprehensive interconnect structure within the series-connected cells [Figure 11A and B][82].

Liu *et al.* employed UV ozone treatment (UVO) and non-thermal annealing to modify MoO_x films (US-MoO_x)[83]. This treatment yielded dense films with elevated energy levels by decomposing $(NH_4)_6Mo_7O_{24}{\cdot}4H_2O$ molecules. The energy levels of the US-MoO_x films were closely aligned with the highest occupied molecular orbital (HOMO) of the active layer, demonstrating high electrical conductivity (850×10^{-3} S cm^{-1}) and low sheet resistance (27 Ω sq^{-1}). The perovskite solar cells (PSCs) based on US-MoO_x exhibited photoelectric conversion efficiency comparable to or exceeding that of E-MoO_x (obtained based on vacuum evaporation MoO_3 powder) films, and surpassed the efficiency of regular PSCs.

Sensors

Surface-enhanced raman scattering (SERS) sensors work by exploiting the significant enhancement of Raman scattering signals that occur when a substance adheres to specific rough metal surfaces or in the proximity of nanoscale metallic particles. This methodology enables the highly sensitive and selective detection of chemical compounds and has extensive applications in the fields of chemistry, biomedicine, and environmental monitoring. In the study conducted by Meng *et al.*, they employed an amorphous monolayer of MoO_3 (a-MoO_3) as the substrate for SERS sensors to detect trace levels of carcinogenic aromatic amines. a-MoO_3 exhibits an LSPR effect within the visible light spectrum, facilitating the plasma-induced hot electron transfer (PIHET) process and thereby enhancing the performance of SERS detection[23].

Two-dimensional nanostructures, characterized by their high surface areas and porosity, endow 2D nanosheets or films with enhanced potential for use in gas sensing applications. Mo-based oxides, which possess various oxidation states and a layered structure, can fine-tune the selectivity for specific gases by altering their chemical composition, morphology, and structure, thereby significantly improving the specificity of gas sensors. Recent research has focused particularly on detecting NO_2[32], NH_3[45], and other harmful gases[26,47]. For instance, 2D Dy_2O_3/MoO_3 heterostructure sensors developed by Ou *et al.* demonstrated a 4.49-fold superior response to 10 ppm NH_3 at a reduced temperature of 328.2 °C, with quicker response/recovery times, 52.6-fold enhanced sensitivity, and a lower detection limit compared to a pure MoO_3 sensor. Moreover, the response of the Dy_2O_3/MoO_3 sensor remains largely unaffected by humidity[25]. Xiao *et al.* designed a porous MoO_3 nanosheet gas sensor for detecting diisopropylamine (DIPA), which exhibited remarkable performance at 217 °C, including an exceptionally high response (30.4 at 10 ppm), a low detection limit (10 ppb), and rapid response times (4.3 s), along with moisture resistance, excellent selectivity, and long-term stability for up to 100 days[29].

Additionally, Jiang *et al.* investigated the utility of 2D MoO_3 for humidity sensing. The MoO_3 derived from liquid-phase exfoliation demonstrated heightened sensitivity (9,794 Ω/RH at 25 °C) and robust stability in humidity detection[84]. Research indicates that the humidity-sensing mechanism of MoO_3 involves electron transfer facilitated by interfacial water molecules. The adsorbed H_2O molecules create a conductive pathway via hydrogen bonding, which diminishes the electron transfer barrier and introduces additional electron states within the valence bands[84].

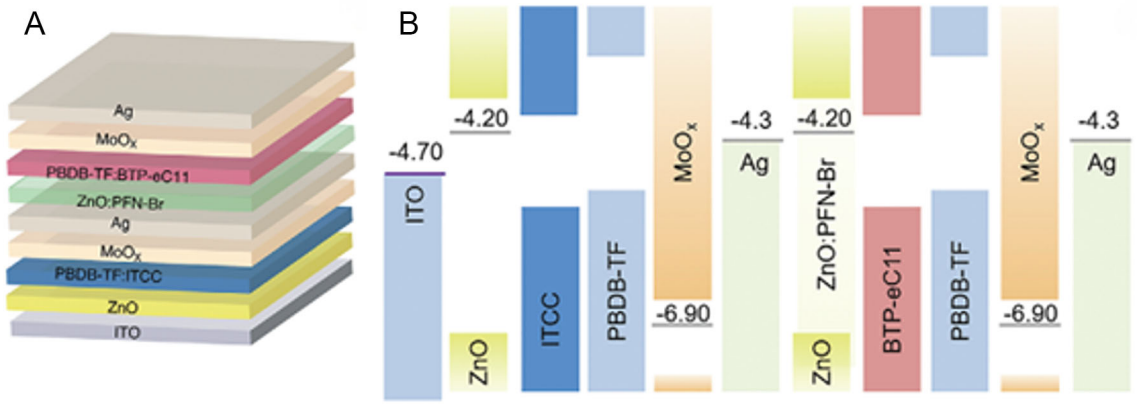

Figure 11. (A) Device structure of tandem cells. (B) Energy level diagram of each layer in tandem cells. All panels reprinted with permission[82].Copyright 2021, Wiley-VCH.

Electrochromism

Electrochromism refers to the reversible change in color or transparency of certain materials when subjected to an electric field. This phenomenon has been harnessed to develop intelligent glass that changes color, garnering significant interest in energy efficiency and environmental conservation. MoO_3, known for its low manufacturing cost, broad light modulation capability, rapid response time, and extended cycle life, serves as an effective electrochromic material. Its electrochromic properties can be further enhanced through doping with other elements[85]. Gao *et al.*, for instance, fabricated tungsten-doped MoO_3 films on Indium Tin oxide (ITO) substrates using electrochemical deposition, as shown in Figure 12[86]. These films exhibited superior electrochromic properties. The layered structure of MoO_3, combined with the incorporation of W atoms to promote efficient W-O-Mo bonding, reduced the switching time from 5.5 to 3.9 s. Moreover, doping increased the optical modulation amplitude by 1.33 times, decreased the coloring and bleaching times to 4.9 and 3.9 s, respectively, and improved the coloring efficiency to 40.43 cm^2 C^{-1}[86].

Kuriakose *et al.*, after successfully isolating 2D MoO_3 nanosheets through liquid phase exfoliation, formulated them into a customizable photochromic MoO_3 ink[21]. This ink, designed according to the Fitzpatrick skin type system, is incorporated into a bio-based elastomer to create an adhesive UV patch. The patch facilitates a qualitative evaluation of UV-A radiation exposure, with its photochromic response under UV light correlating to a calculated minimum erythema dose (MED). This feature offers visual cues to users, assisting them in avoiding excessive exposure and protecting their skin from damage.

Electronic and optoelectronic devices

Two-dimensional monolayer MoO_3, with a work function of approximately 6.9 eV, is well-suited for electronic and optoelectronic applications[87]. It serves as an effective interface modification layer, addressing the issue of high contact resistance at the metal-organic interface in organic thin-film transistors (OTFTs). However, its propensity to diffuse into organic semiconductors (OSCs) can compromise device stability. Yang *et al.* mitigated MoO_3 diffusion by creating high-density organic barrier layer (OBL) films on the OSC active layer[88]. These interlayer materials (IMLs) not only reduced contact resistance and prevented minority carrier injection into the OTFT channel but also enhanced device stability and the on/off current ratio.

Shan *et al.* developed a memristor utilizing an α-MoO_3 cross-point structure, which exhibited superior electrical characteristics, including endurance over 103 cycles, a switching ratio (R_{OFF}/R_{ON}) exceeding 104, multilevel storage capability, and a fast response time of 10 μs[89]. Hong *et al.* discovered that ultra-thin α-

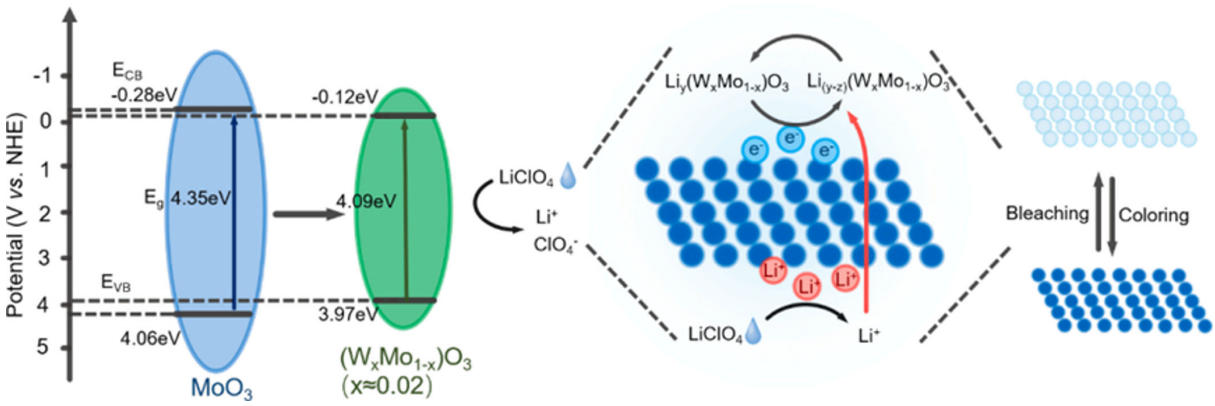

Figure 12. Mechanism underlying the electrochromism of W-doped molybdenum oxide films. Reprinted with permission[86]. Copyright 2023, Elsevier.

MoO_3 memristors with silver/graphene electrodes achieved a high on/off ratio of approximately 104, a low set voltage of about 0.5 V, a long retention time exceeding 104 s, and excellent repeatability in over 150 voltage cycle scans[35]. These studies indicate that 2D MoO_3 is a promising material for post-Moore era memristors.

Xu *et al.* demonstrated that MoO_3 films possess excellent photoelectric synaptic functionality, capable of simulating long-term potentiation (LTP) and long-term depression (LTD) processes under near-infrared light[37]. They also highlighted the potential of MoO_3 films in advanced optoelectronic systems, particularly their unique ability to simulate image processing functions. Lee *et al.* fabricated a hybrid photodetector by coating $CsPbBr_3$ quantum dots onto 2D MoO_3 nanomaterials, resulting in a significantly improved photocurrent response across the UV to visible light spectrum[39].

CONCLUSIONS

This article systematically reviews the synthesis, structural modulation, and applications of 2D Mo-based oxides, specifically highlighting recent advances in MoO_3 and MoO_2, as well as substoichiometric MoO_{3-x} and MoO_{2-x}. Through a comprehensive summary of existing research, it is not difficult to see that the microstructure critically influences the performance of 2D Mo-based oxides, with various structural regulation techniques significantly affecting their electrical, optical, and catalytic properties. Therefore, it is imperative to consider these microscopic characteristics when designing new materials. The use of advanced digital technologies such as computational simulations and machine learning tools can help discover or understand novel materials or structures. This approach not only accelerates the design process of new materials but also aids in elucidating complex physical and chemical mechanisms. With the recognition of these technologies by the 2024 Nobel Prizes in Physics and Chemistry, we believe this will be a significant trend in future materials science development. Indeed, we are pleased to observe ongoing efforts in this direction concerning 2D Mo-based oxides[79,90].

It is worth noting that numerous studies have focused on the properties and applications of Mo-based oxides at low dimensional scales, especially monolayer Mo-based oxides[91]. Thanks to research into exotic properties of monolayer Mo-based oxides, such as surface plasmon resonance effects, twistronics, and chirality, will facilitate the development of new electronic and optoelectronic devices[92]. In addition, MoO_{3-x} is beginning to show promise in emerging fields such as catalysis and sensors, indicating broad prospects for defect-rich Mo-based oxides[93,94].

Lastly, the methods for synthesizing Mo-based oxides and the underlying mechanisms for their regulation remain incompletely understood. The efficient preparation of high-quality 2D Mo-based oxides with specific properties remains an open question that requires further experimental and theoretical investigation. These works are also pertinent to the study of other 2D metal oxides. Research in 2D materials continues to offer many exciting opportunities for those engaged in scientific endeavors. As part of this field, Mo-based oxides will play a crucial role and usher in new developments.

DECLARATIONS

Authors' contributions

Conceived and designed the study, conducted literature search and organized references: Zhao, Z.; Zhou, T.; Xiong, L.

Prepared the samples and collected the data, performed data analysis and wrote the main draft of the paper: Zhao, Z.; Zhou, T.; Lei, W.; Chen, K.; Tian, K.; Xiong, G.

Provided technical and material support, advised on scientific discussion and manuscript revision: Xiong, L., Kuang, S.; Yu, Y.; Huang, L.

All authors participated in the writing of the manuscript.

Availability of data and materials

Not applicable.

Financial support and sponsorship

This work was partially supported by the "Key Project of Science and Technology Research Program of Hubei Provincial Department of Education" [F2023008], the "Youth Project of Natural Science Foundation of Hubei Province" [Grant No. 2023AFB224], and the "Science Foundation of Wuhan Institute of Technology" [Grant No. 22QD29].

Conflicts of interest

Prof. Huang, L. is Guest Editor of the Special Issue *Structural Regulation and Application of Two-Dimensional Metal Oxide* of the journal *Microstructures*; Prof. Yu, Y. and Prof. Xiong, L. are Assistant Guest Editors of the Special Issue of the journal *Microstructures*. They were not involved in any steps of editorial processing, notably including reviewer selection, manuscript handling, or decision-making, while the other authors have declared that they have no conflicts of interest.

Ethical approval and consent to participate

Not applicable.

Consent for publication

Not applicable.

REFERENCES

1. Gusain, R.; Gupta, K.; Joshi, P.; Khatri, O. P. Adsorptive removal and photocatalytic degradation of organic pollutants using metal oxides and their composites: a comprehensive review. *Adv. Colloid. Interface. Sci.* **2019**, *272*, 102009. DOI PubMed
2. Mei, J.; Liao, T.; Kou, L.; Sun, Z. Two-dimensional metal oxide nanomaterials for next-generation rechargeable batteries. *Adv. Mater.* **2017**, *29*, 1700176. DOI
3. Zhu, Y.; Peng, L.; Fang, Z.; Yan, C.; Zhang, X.; Yu, G. Structural engineering of 2D nanomaterials for energy storage and catalysis. *Adv. Mater.* **2018**, *30*, e1706347. DOI

4. Garland, B. M.; Fairley, N.; Strandwitz, N. C.; Thorpe, R.; Bargiela, P.; Baltrusaitis, J. A study of in situ reduction of MoO_3 to MoO_2 by X-ray photoelectron spectroscopy. *Appl. Surf. Sci.* **2022**, *598*, 153827. DOI
5. de Castro, I. A.; Datta, R. S.; Ou, J. Z.; et al. Molybdenum oxides - from fundamentals to functionality. *Adv. Mater.* **2017**, *29*, 1701619. DOI
6. Zou, B.; Wang, X.; Zhou, Y.; et al. Optical effect modulation in polarized raman spectroscopy of transparent layered α-MoO_3. *Small* **2023**, *19*, e2206932. DOI
7. Ye, M.; Qiang, B.; Zhu, S.; et al. Nano-optical engineering of anisotropic phonon resonances in a hyperbolic α-MoO_3 metamaterial. *Adv. Opt. Mater.* **2022**, *10*, 2102096. DOI
8. Tao, S.; Hou, T.; Zeng, Y.; et al. Anisotropic Fermat's principle for controlling hyperbolic van der Waals polaritons. *Photon. Res.* **2022**, *10*, B14. DOI
9. Wang, Y.; Guo, X.; You, S.; et al. Giant quartic-phonon decay in PVD-grown α-MoO_3 flakes. *Nano. Res.* **2023**, *16*, 1115-22. DOI
10. Zheng, M.; Liu, P.; Yan, P.; et al. Heterogeneous CNF/MoO_3 nanofluidic membranes with tunable surface plasmon resonances for solar-osmotic energy conversion. *Mater. Horiz.* **2024**, *11*, 3375-85. DOI
11. Kong, W.; Liu, W.; Zheng, X.; Xu, Q. Sunlight driven reversible and tunable plasmon resonance in 2D amorphous molybdenum oxide. *Adv. Opt. Mater.* **2024**, *12*, 2301821. DOI
12. Hu, G.; Ou, Q.; Si, G.; et al. Topological polaritons and photonic magic angles in twisted α-MoO_3 bilayers. *Nature* **2020**, *582*, 209-13. DOI
13. Wang, S. Y.; Li, D. K.; Zha, M. J.; Yan, X. Q.; Liu, Z.; Tian, J. Tunable optical activity in twisted anisotropic two-dimensional materials. *ACS. Nano.* **2023**, *17*, 16230-8. DOI
14. Duan, J.; Álvarez-Pérez, G.; Lanza, C.; et al. Multiple and spectrally robust photonic magic angles in reconfigurable α-MoO_3 trilayers. *Nat. Mater.* **2023**, *22*, 867-72. DOI
15. Liu, H.; Yu, K.; Zhang, K.; Ai, Q.; Xie, M.; Wu, X. Effect of substrate on the near-field radiative heat transfer between α-MoO_3 films. *Int. J. Heat. Mass. Transf.* **2023**, *210*, 124206. DOI
16. Li, L.; Wu, X.; Liu, H.; Shi, K.; Liu, Y.; Yu, K. Near-field radiative modulator based on α-MoO_3 films. *Int. J. Heat. Mass. Transfer.* **2023**, *216*, 124603. DOI
17. Ren, H.; Sun, S.; Cui, J.; Li, X. Synthesis, functional modifications, and diversified applications of molybdenum oxides micro-/nanocrystals: a review. *Cryst. Growth. Des.* **2018**, *18*, 6326-69. DOI
18. Scanlon, D. O.; Watson, G. W.; Payne, D. J.; Atkinson, G. R.; Egdell, R. G.; Law, D. S. L. Theoretical and experimental study of the electronic structures of MoO_3 and MoO_2. *J. Phys. Chem. C.* **2010**, *114*, 4636-45. DOI
19. Huang, C.; Zhang, W.; Zheng, W. The debut and spreading the landscape for excellent vacancies-promoted electrochemical energy storage of nano-architected molybdenum oxides. *Mater. Today. Energy.* **2022**, *30*, 101154. DOI
20. Xie, H.; Li, Z.; Cheng, L.; et al. Recent advances in the fabrication of 2D metal oxides. *iScience* **2022**, *25*, 103598. DOI PubMed PMC
21. Kuriakose, S.; Kayani, A. B. A.; Monshipouri, M.; et al. Customized two-dimensional nanostructured MoO_3 inks for spectrally selective UV chromic patches. *ACS. Appl. Nano. Mater.* **2022**, *5*, 18553-60. DOI
22. Wei, Z.; Gasparyan, M.; Liu, L.; et al. Microwave-exfoliated 2D oligo-layer MoO_{3-x} nanosheets with outstanding molecular adsorptivity and room-temperature gas sensitivity on ppb level. *Chem. Eng. J.* **2023**, *454*, 140076. DOI
23. Meng, X.; Yu, J.; Shi, W.; et al. SERS detection of trace carcinogenic aromatic amines based on amorphous MoO_3 monolayers. *Angew. Chem. Int. Ed.* **2024**, *63*, e202407597. DOI
24. Wu, T.; Zhang, F.; Wang, J.; Liu, X.; Tian, Y.; Chu, K. Electrochemical reduction of nitrite to ammonia on amorphous MoO_3 nanosheets. *Dalton. Trans.* **2024**, *53*, 877-81. DOI
25. Ou, Y.; Zhou, Y.; Guo, Y.; et al. 2D/2D Dy_2O_3 nanosheet/MoO_3 nanoflake heterostructures for humidity-independent and sensitive ammonia detection. *ACS. Sens.* **2023**, *8*, 4253-63. DOI
26. Pradeep Kumar, P.; Singh, V. Enhanced dual gas sensing performance of MoS_2/MoO_3 nanostructures for NH_3 and NO_2 detection. *Ceram. Int.* **2024**, *50*, 21978-88. DOI
27. Wang, Z. Y.; Yuan, B.; Zhang, F. G.; et al. Photocatalytic nitrogen fixation coupled with the generation of value-added chemicals from N_2 and cellulose over MoO_3 nanosheets. *Inorg. Chem.* **2024**, *63*, 9715-9. DOI
28. Ding, W.; Li, X.; Su, S.; et al. In-situ construction of Schottky junctions with synergistic interaction of oxygen vacancies in Mo@MoO_3 nanosheets for efficient N_2 photoreduction. *Appl. Surf. Sci.* **2023**, *633*, 157594. DOI
29. Xiao, R.; Wang, T.; Feng, S.; et al. Porous MoO_3 nanosheets for conductometric gas sensors to detect diisopropylamine. *Sens. Actuators. B. Chem.* **2023**, *382*, 133472. DOI
30. Madani, S.; Tesfamichael, T.; Motta, N.; Wang, H. Simulation of perovskite solar cells using molybdenum oxide thin films as interfacial layer for enhancing device performance. *Sustain. Mater. Technol.* **2022**, *32*, e00426. DOI
31. Du, Y.; Li, G.; Peterson, E. W.; et al. Iso-oriented monolayer α-MoO_3(010) films epitaxially grown on $SrTiO_3$(001). *Nanoscale* **2016**, *8*, 3119-24. DOI
32. Bisht, P.; Kumar, A.; Jensen, I. T.; Ahmad, M.; Belle, B. D.; Mehta, B. Enhanced gas sensing response for 2D α-MoO_3 layers: thickness-dependent changes in defect concentration, surface oxygen adsorption, and metal-metal oxide contact. *Sens. Actuators. B. Chem.* **2021**, *341*, 129953. DOI
33. Zhao, X.; Chu, Q.; Guo, S.; et al. Controllable hot electron transfer in the Ag/MoO_3 layer by layer system: thickness-dependent MoO_3

layer. *Spectrochim. Acta. A. Mol. Biomol. Spectrosc.* **2023**, *286*, 121995. DOI

34. Rahman, M.; Chetri, S.; Pemmaraju, D. B.; Murty, U. S.; Deshpande, U. P.; Kakati, M. An expanded plasma jet assisted technique for very high-rate synthesis of 2D α-MoO_3 nanomaterials, with surface oxygen vacancies and robust induced ferromagnetism. *Vacuum* **2024**, *225*, 113237. DOI
35. Hong, Y.; Lan, S.; Pan, B.; et al. Thinner 2D α-MoO_3 makes setting up memristors easier. *J. Materiomics.* **2024**, *10*, 1279-89. DOI
36. Deng, L.; Zhang, Q.; Li, W.; et al. KCl acts as a flux to assist the growth of sub-millimeter-scale metallic 2D non-layered molybdenum dioxide. *Rare. Met.* **2025**, *44*, 404-16. DOI
37. Xu, H.; Karbalaei, A. M.; Wang, S.; et al. Tunability of near infrared opto-synaptic properties of thin MoO_3 films fabricated by atomic layer deposition. *Appl. Surf. Sci.* **2022**, *593*, 153399. DOI
38. Kim, Y. W.; Park, J.; Park, J. H.; et al. Self-isolating electrode deposition process using the area-selective MoO_2 and MoO_3 atomic layer deposition technique. *Appl. Mater. Today.* **2024**, *37*, 102160. DOI
39. Lee, D. J.; Kumar, G. M.; Kim, Y.; et al. Hybrid $CsPbBr_3$ quantum dots decorated two dimensional MoO_3 nanosheets photodetectors with enhanced performance. *J. Mater. Res. Technol.* **2022**, *18*, 4946-55. DOI
40. Kundu, M.; Mondal, D.; Mondal, I.; et al. A rational preparation strategy of phase tuned MoO_3 nanostructures for high-performance all-solid asymmetric supercapacitor. *J. Energy. Chem.* **2023**, *87*, 192-206. DOI
41. Zhu, Y.; Tan, Y.; Li, H. MoO_3 nanoplates preparation via self-sacrifice C_3N_4 for supercapacitors in an acid electrolyte. *J. Energy. Storage.* **2023**, *60*, 106657. DOI
42. Alam, M. H.; Chowdhury, S.; Roy, A.; et al. Wafer-scalable single-layer amorphous molybdenum trioxide. *ACS. Nano.* **2022**, *16*, 3756-67. DOI
43. Liu, B.; Wu, S.; Lv, Y.; et al. Facile synthesis of oxygen-deficient MoO_{3-x} nanosheets by light radiation for fast electrochromic supercapacitors. *Electrochim. Acta.* **2023**, *464*, 142894. DOI
44. Qi, S.; Liu, G.; Zhang, K.; Chen, J.; Zhao, Y.; Lou, Y. Colloidal synthesis of plasmonic ultrathin transition-metal oxide nanosheets. *ACS. Sustain. Chem. Eng.* **2022**, *10*, 9565-72. DOI
45. Shkir, M.; Ben, G. T. A.; Alkallas, F. H.; Alfaify, S. High performance of the rare earth (Er, Gd & Pr) doped MoO_3 thin films for advanced applications towards ammonia gas sensing. *J. Mater. Res. Technol.* **2022**, *20*, 4556-65. DOI
46. Li, T.; Zhu, L.; Lu, L.; et al. Highly sensitive optical fiber plasmonic sensors by integrating hydrogen doped molybdenum oxide. *IEEE. Sensors. J.* **2022**, *22*, 7734-42. DOI
47. Li, W.; Xu, H.; Wang, A.; et al. Insitu controllable synthesis of MoO_3 nanoflakes and its temperature-dependent dual selectivity for detection of ethanol and isopropanol. *Sens. Actuators. B. Chem.* **2024**, *408*, 135548. DOI
48. Kriegel, I.; Jiang, C.; Rodríguez-Fernández, J.; et al. Tuning the excitonic and plasmonic properties of copper chalcogenide nanocrystals. *J. Am. Chem. Soc.* **2012**, *134*, 1583-90. DOI
49. Li, C.; Jang, H.; Kim, M. G.; Hou, L.; Liu, X.; Cho, J. Ru-incorporated oxygen-vacancy-enriched MoO_2 electrocatalysts for hydrogen evolution reaction. *Appl. Catal. B. Environ.* **2022**, *307*, 121204. DOI
50. Luo, Z.; Miao, R.; Huan, T. D.; et al. Mesoporous MoO_{3-x} material as an efficient electrocatalyst for hydrogen evolution reactions. *Adv. Energy. Mater.* **2016**, *6*, 1600528. DOI
51. Cheng, H.; Kamegawa, T.; Mori, K.; Yamashita, H. Surfactant-free nonaqueous synthesis of plasmonic molybdenum oxide nanosheets with enhanced catalytic activity for hydrogen generation from ammonia borane under visible light. *Angew. Chem. Int. Ed.* **2014**, *53*, 2910-4. DOI PubMed
52. Sun, Y.; Cui, J.; Wang, C.; Fu, S.; Sun, S.; Wang, X. Controllable synthesis of defect-enriched MoO_3 for enhanced H_2S sensing through hydrothermal methods: experiments and DFT calculations. *J. Alloys. Compd.* **2023**, *968*, 172035. DOI
53. Sun, J.; Qin, S.; Zhao, Z.; Zhang, Z.; Meng, X. Rapid carbothermal shocking fabrication of iron-incorporated molybdenum oxide with heterogeneous spin states for enhanced overall water/seawater splitting. *Mater. Horiz.* **2024**, *11*, 1199-211. DOI
54. Xu, L.; Zhou, W.; Chao, S.; et al. Advanced oxygen-vacancy Ce-doped MoO_3 ultrathin nanoflakes anode materials used as asymmetric supercapacitors with ultrahigh energy density. *Adv. Energy. Mater.* **2022**, *12*, 2200101. DOI
55. Lin, Y.; Zhang, Y.; Magomedov, A.; et al. 18.73% efficient and stable inverted organic photovoltaics featuring a hybrid hole-extraction layer. *Mater. Horiz.* **2023**, *10*, 1292-300. DOI
56. Wang, H.; Guan, N.; Feng, Z.; Xiang, W.; Zhao, H.; Zhang, X. Constructing defect engineered 2D/2D MoO_3/g-C_3N_4 Z-scheme heterojunction for enhanced photocatalytic activity. *J. Alloys. Compd.* **2022**, *926*, 166964. DOI
57. Peng, J.; Shen, J.; Yu, X.; Tang, H.; Zulfiqar; Liu, Q. Construction of LSPR-enhanced 0D/2D CdS/MoO_{3-x} S-scheme heterojunctions for visible-light-driven photocatalytic H_2 evolution. *Chin. J. Catal.* **2021**, *42*, 87-96. DOI
58. Wei, Y.; Zhang, Q.; Zhou, Y.; et al. Noble-metal-free plasmonic MoO_{3-x}-based S-scheme heterojunction for photocatalytic dehydrogenation of benzyl alcohol to storable H_2 fuel and benzaldehyde. *Chin. J. Catal.* **2022**, *43*, 2665-77. DOI
59. Wang, H.; Liu, Q.; Xu, M.; et al. Dual-plasma enhanced 2D/2D/2D g-C_3N_4/Pd/MoO_{3-x} S-scheme heterojunction for high-selectivity photocatalytic CO_2 reduction. *Appl. Surf. Sci.* **2023**, *640*, 158420. DOI
60. Yoon, A.; Kim, J. H.; Yoon, J.; Lee, Y.; Lee, Z. van der Waals epitaxial formation of atomic layered α-MoO_3 on MoS_2 by oxidation. *ACS. Appl. Mater. Interfaces.* **2020**, *12*, 22029-36. DOI
61. Krishnan, A.; Kamaraj, M.; Nayak, P. K.; Ramaprabhu, S. Surface functionalized 2D MoO_3-hBN heterostructure as friction modifiers in boundary lubrication regime. *Surf. Interfaces.* **2024**, *51*, 104527. DOI
62. Wang, Q.; Tian, H.; Zhang, Z.; et al. Keggin-type polycationic $AlO_4Al_{12}(OH)_{24}(H_2O)_{12}^{7+}$ intercalated MoO_3 composites for methyl

orange adsorption. *Chin. Chem. Lett.* **2022**, *33*, 2617-20. DOI

63. Tan, Y.; He, J.; Wang, B.; Li, C. C.; Wang, T. Tuning the layer structure of molybdenum trioxide towards high-performance aqueous zinc-ion batteries. *Chin. Chem. Lett.* **2023**, *34*, 107410. DOI
64. Gao, Z.; Tan, R.; Pan, Z.; et al. Boosting ammonia synthesis over MoO_2 by Li intercalation. *Green. Chem.* **2022**, *24*, 7584-91. DOI
65. Reed, B. W.; Chen, E.; Koski, K. J. Tunable chemochromism and elastic properties in intercalated MoO_3: Au-, Cr-, Fe-, Ge-, Mn-, and Ni-MoO_3. *ACS. Nano.* **2024**, *18*, 12845-52. DOI
66. Hu, T.; Xue, B.; Meng, F.; et al. Preparation of 2D Polyaniline/MoO_{3-x} superlattice nanosheets via intercalation-induced morphological transformation for efficient chemodynamic therapy. *Adv. Healthc. Mater.* **2023**, *12*, e2202911. DOI
67. Xie, S.; Cheng, X.; Hu, C.; et al. Pressure effect on structure transition and optical anisotropy in MoO_3. *Appl. Phys. Lett.* **2022**, *120*, 131901. DOI
68. Wang, S.; Wang, Y.; Liu, T.; Wang, L.; Huang, Y.; Lu, Y. Irreversible pressure effect on phase transitions and bandgap narrowing of layered MoO_3. *Mater. Today. Adv.* **2024**, *21*, 100476. DOI
69. Chia, X.; Pumera, M. Characteristics and performance of two-dimensional materials for electrocatalysis. *Nat. Catal.* **2018**, *1*, 909-21. DOI
70. Wen, K.; Huang, L.; Qu, L.; et al. g-C_3N_4/MoO_3 composite with optimized crystal face: a synergistic adsorption-catalysis for boosting cathode performance of lithium-sulfur batteries. *J. Colloid. Interface. Sci.* **2023**, *649*, 890-9. DOI
71. Hsu, F. H.; Hsu, S. Y.; Subramani, R.; et al. The ion behavior and storage mechanism of 2D MoO_3 layer structure in an air-stable hydrated eutectic electrolyte for aluminum-ion energy storage. *J. Energy. Storage.* **2024**, *84*, 110693. DOI
72. Hao, L.; Huang, H.; Zhang, Y.; Ma, T. Oxygen vacant semiconductor photocatalysts. *Adv. Funct. Mater.* **2021**, *31*, 2100919. DOI
73. Ashraf, G. A.; Rasool, R. T.; Rasool, R. U.; et al. Photocatalytic stimulation of peroxymonosulfate by novel MoO_3@ZrO_2 with Z-scheme heterojunction for diclofenac sodium degradation. *J. Water. Process. Eng.* **2023**, *51*, 103435. DOI
74. Wang, J.; Tao, J.; Dong, X.; et al. Hydrothermal oxygen uncoupling of high-concentration biogas slurry over Cu-α-Fe_2O_3·α-MoO_3 catalyst. *J. Environ. Manag.* **2022**, *320*, 115827. DOI
75. Zhao, X.; Zhou, W.; Xu, L.; et al. Oxygen-vacancy Ce-MoO_3 nanosheets loaded Pt nanoparticles for super-efficient photoelectrocatalytic oxidation of methanol. *Appl. Surf. Sci.* **2024**, *655*, 159576. DOI
76. Zhu, Y.; Lin, Q.; Zhong, Y.; Tahini, H. A.; Shao, Z.; Wang, H. Metal oxide-based materials as an emerging family of hydrogen evolution electrocatalysts. *Energy. Environ. Sci.* **2020**, *13*, 3361-92. DOI
77. Wang, X.; Liu, G.; Zhang, D.; et al. N-doped carbon sheets supported P-Fe_3O_4-MoO_2 for freshwater and seawater electrolysis. *J. Colloid. Interface. Sci.* **2023**, *652*, 1217-27. DOI
78. Li, J.; Cheng, Y.; Zhang, J.; Fu, J.; Yan, W.; Xu, Q. Confining Pd nanoparticles and atomically dispersed Pd into defective MoO_3 nanosheet for enhancing electro- and photocatalytic hydrogen evolution performances. *ACS. Appl. Mater. Interfaces.* **2019**, *11*, 27798-804. DOI
79. Deka, H.; Sunaniya, A. K.; Agarwal, P. Simulation studies on MoS_2 (n)/a-Si:H (i)/c-Si (p)/MoO_3 heterojunction solar cells using one sided short diode approximation. *Solar. Energy.* **2023**, *263*, 111943. DOI
80. Li, J.; Kang, Q.; Wang, Y.; et al. Low oxygen content MoO_x and SiO_x tunnel layer based heterocontacts for efficient and stable crystalline silicon solar cells approaching 22% efficiency. *Adv. Funct. Mater.* **2024**, *34*, 2310619. DOI
81. Suzuki, I.; Lin, Z.; Nogami, T.; et al. High open-circuit voltage in single-crystalline *n* -type SnS/MoO_3 photovoltaics. *APL. Mater.* **2023**, *11*, 031116. DOI
82. Wang, J.; Zheng, Z.; Zu, Y.; et al. A tandem organic photovoltaic cell with 19.6% efficiency enabled by light distribution control. *Adv. Mater.* **2021**, *33*, e2102787. DOI
83. Liu, Z.; Zhang, H.; Sun, L. Enhanced performance of polymer solar cells by ultraviolet-ozone treatment of MoO_x films with non-thermal annealing treatment of MoO_x films. *Surf. Interfaces.* **2024**, *51*, 104701. DOI
84. Jiang, W.; Su, M.; Zheng, Y.; Fei, T. Efficient electron transfer through interfacial water molecules across two-dimensional MoO_3 for humidity sensing. *ACS. Appl. Mater. Interfaces.* **2024**, *16*, 7406-14. DOI
85. Zhang, W.; Li, H.; Hopmann, E.; Elezzabi, A. Y. Nanostructured inorganic electrochromic materials for light applications. *Nanophotonics* **2020**, *10*, 825-50. DOI
86. Gao, G.; Tao, X.; He, Y.; et al. Electrochromic composites films composed of MoO_3 doped by tungsten atoms with remarkable response speed and color rendering efficiency via electrochemical deposition. *Appl. Surf. Sci.* **2023**, *640*, 158346. DOI
87. Kowalczyk, D. A.; Rogala, M.; Szałowski, K.; et al. Two-dimensional crystals as a buffer layer for high work function applications: the case of monolayer MoO_3. *ACS. Appl. Mater. Interfaces.* **2022**, *14*, 44506-15. DOI PubMed PMC
88. Yang, Z.; Guo, C.; Qin, L.; et al. Enhanced organic thin-film transistor stability by preventing MoO_3 diffusion with metal/MoO_3/organic multilayered interface source-drain contact. *ACS. Appl. Mater. Interfaces.* **2023**, *15*, 1704-17. DOI
89. Shan, X.; Liu, P.; Wang, F.; et al. Dual-conductivity mechanism investigation of 2D α-MoO_3-based multi-level memristor. *Sci. China. Mater.* **2023**, *66*, 4773-81. DOI
90. Ma, Y.; Lang, J. 2D SnO/MoO_3 van der Waals heterojunction with tunable electronic behavior for multifunctional applications: DFT calculations. *App. Surf. Sci.* **2023**, *611*, 155719. DOI
91. Surnev, S.; Netzer, F. P. Tungsten and molybdenum oxide nanostructures: two-dimensional layers and nanoclusters. *J. Phys. Condens. Matter.* **2022**, *34*, 233001. DOI PubMed
92. Petronijevic, E.; Dereshgi, S. A.; Larciprete, M. C.; Centini, M.; Sibilia, C.; Aydin, K. Extrinsic chirality and circular dichroism at

visible frequencies enabled by birefringent α-MoO_3 nanoscale-thick films: implications for chiro-optical control. *ACS. Appl. Nano. Mater.* **2022**, *5*, 5609-16. DOI

93. Kundu, M.; Mondal, D.; Bose, N.; Basu, R.; Das, S. 2D MoO_3/PVDF-HFP nanocomposites for flexible piezoelectric nanogenerator and wireless mechanosensor applications. *ACS. Appl. Nano. Mater.* **2024**, *7*, 1804-14. DOI
94. Novotný, P.; Yusuf, S.; Li, F.; Lamb, H. H. MoO_3/Al_2O_3 catalysts for chemical-looping oxidative dehydrogenation of ethane. *J. Chem. Phys.* **2020**, *152*, 044713. DOI